ACS APPLIED MATERIALS & INTERFACES

www.acsami.org
Research Article

Self-Healing Scaffolding Technology with Strong, Reversible Interactions under Physiological Conditions for Engineering Marbled Cultured Meat

Lam Tan Hao, Seunghyeon Lee, Dong Soo Hwang, Hyeonyeol Jeon, Jeyoung Park,* Hyo Jeong Kim,* and Dongyeop X. Oh*

Cite This: ACS Appl. Mater. Interfaces 2025, 17, 31881−31897
Read Online

ABSTRACT: Cultured meat offers a sustainable alternative to animal farming, with the potential to reduce environmental impacts and improve food security. However, recapitulating natural meat marbling remains a significant challenge. This study presents a straightforward technology for achieving precise marbling patterns in large-scale cultured meat using self-healing hydrogels containing boronic acid-conjugated chitosan. Unlike conventional hydrogels, which require nonphysiological conditions for strong, reversible bonding, our system achieves robust reversible bonding at neutral pH through a unique mechanism: the nucleophilic groups of chitosan facilitate boronic acid−diol bond formation, exhibiting half the strength of a typical covalent bond, as demonstrated by nanomechanics analysis. The hydrogels form dual reversible networks of boronic acid−diol and hydrogen bonds, enabling self-healing and tunable stiffness. Biocompatibility studies confirm that they support the growth of mouse-derived cells and bovine-derived primary muscle cells. Each hydrogel variant optimizes mechanotransduction for the distinct requirements of fat or muscle cell culture and differentiation. This self-healing scaffolding technology enables the seamless assembly of muscle and fat monocultures into centimeter-thick meat with micrometer-scale marbling patterns, tailoring organoleptic properties and nutritional profiles without the need for meat glues or processing equipment.

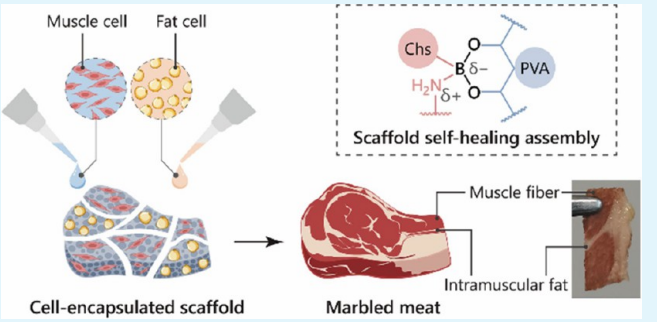

KEYWORDS: *cultured meat, self-healing, hydrogel, chitosan, boronic acid, marbled meat*

1. INTRODUCTION

Meat is a vital source of nutrients for humans and a key component of global cuisines.[1] The sensory appeal of meat, especially red meat, is largely attributed to marbling, which refers to the distribution of intramuscular fat.[2] Marbling degree is a widely used visual indicator of palatability in major beef-quality grading systems, including the US Department of Agriculture (USDA) Prime, Japanese Wagyu, and Korean Hanwoo.[3] Despite its increasing demand, global meat production still heavily relies on animal farming, which poses significant challenges related to the environment, public health, and animal welfare.[4] To address these challenges, scientists have been investigating cultured meat, which is produced by cultivating animal cells in vitro using stem-cell biology and tissue engineering. Cultured meat aligns with the United Nations Sustainable Development Goals and offers a potential solution to dietary, ethical, and cultural concerns associated with conventional meat.[5,6]

Despite advances in whole-muscle cultured meat production, replicating natural marbling in large-scale meat constructs to enhance consumer appeal remains a challenge.[7−10] Two primary technologies have been adopted: (1) coculturing and differentiating fat and muscle cells, and (2) monoculturing these cells and assembling them to emulate natural marbling.[11] However, their successful implementation remains limited. Coculturing presents difficulties in managing cell-type ratios and ensuring their simultaneous growth and differentiation.[12] Additionally, the postassembly approach suffers from insufficient adhesion between monocultures and the lack of extrudable scaffolds for processing cell assemblies (Figure 1).[13,14]

Scaffolds, a central component of cultured meat, are often based on hydrogels that mimic the natural extracellular matrix (ECM).[15] Various hydrogel materials have been investigated for use in meat culture. Protein-based hydrogels effectively

Received: February 19, 2025
Revised: April 10, 2025
Accepted: April 24, 2025
Published: May 3, 2025

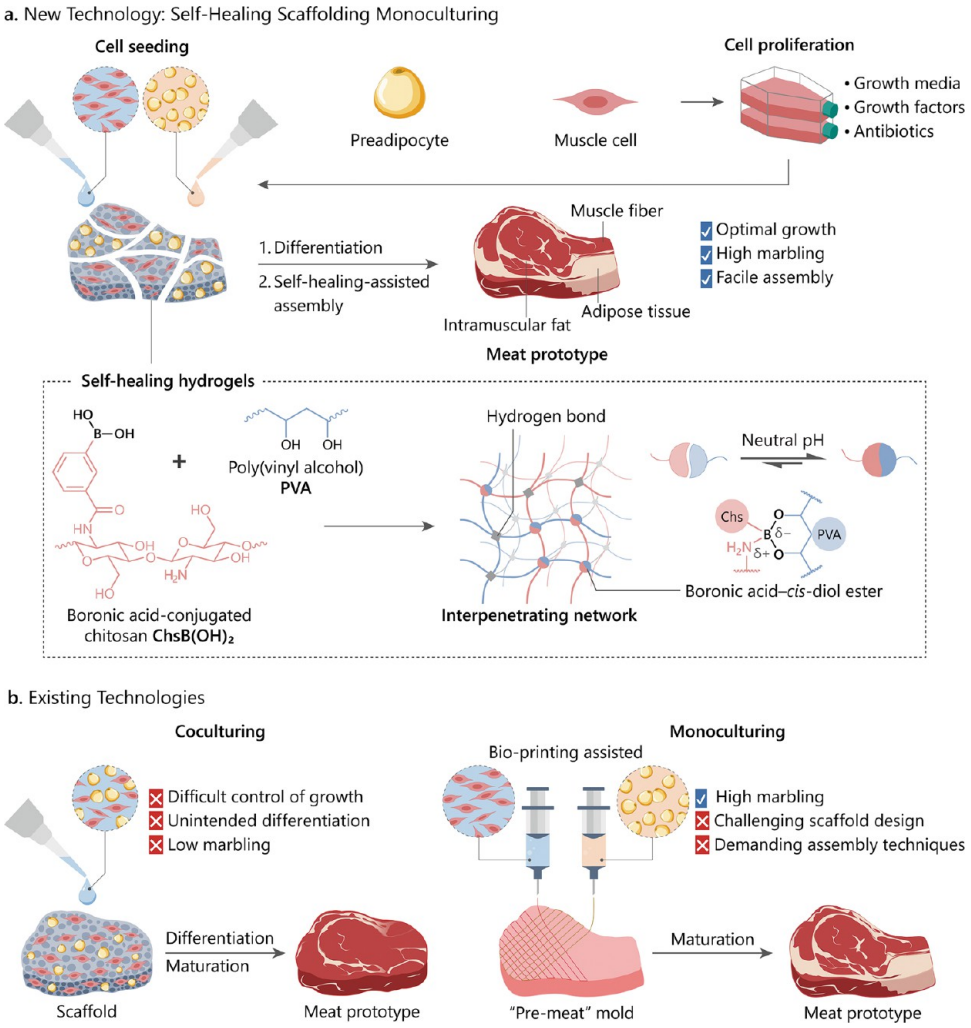

Figure 1. Self-healing scaffolding technology for culturing marbled meat. (a) Meat prototype with customized marbling is constructed using interpenetrating-network hydrogels comprising boronic acid-conjugated chitosan [ChsB(OH)$_2$] (orange) and poly(vinyl alcohol) (PVA) (blue), which are capable of self-healing through boronic acid−*cis*-diol ester linkages and are mechanically reinforced through hydrogen bonds. Coordination between chitosan-nitrogen and boron atoms facilitates ester bond formation at physiological pH. Preadipocytes and muscle cells proliferate and differentiate into fat and muscle tissue, respectively, and are subsequently assembled into a meat prototype via the self-healing ability of the hydrogel without the need for external adhesives or devices. (b) Self-healing scaffolding technology overcomes challenges associated with coculture and monoculture approaches for cultivating meat.

support cell attachment but are limited by the lack of low-cost, scalable sources. Synthetic polymer hydrogels require a careful evaluation of their reagents and degradation profiles to ensure safe consumption. Biomass-derived hydrogels often pose challenges in terms of their fabrication and scalability.[16] Regardless of the material, conventional hydrogels typically lack sufficient adhesion to form intricately marbled structures and require mechanical strength optimization for specific cell types to support proper differentiation.[16,17]

Inspired by the self-healing ability of living organisms, researchers have developed synthetic materials that can autonomously repair damage.[18] Self-healing hydrogels are particularly valuable in tissue engineering, as their physico-chemical properties play pivotal roles in regulating cell growth and differentiation. They also facilitate seamless bridging between tissue layers in biothree-dimensional (3D) printing.[17] Self-healing is achieved through reversible interactions, including physical cross-links or dynamic covalent bonds.[19,20] The latter maintain both the structural integrity of covalently cross-linked systems and the flexibility of physically cross-linked systems, which is advantageous in physiological environments where hydration and metal-ion complexation screen molecular interactions.[21]

One example of dynamic covalent bonds used for cross-linking hydrogels is the cyclic ester bond between boronic acids and 1,2- or 1,3-*cis*-diols, with a bonding equilibrium dependent on the solution pH and pK_a of the boronic acid, which is typically greater than 7.4 (physiological pH). A pH above the pK_a favors ester bond formation, whereas a pH below the pK_a promotes bond dissociation.[22,23] However, alkaline conditions limit its adaptability in cell culture. Attempts to stabilize these interactions under physiological conditions by coordination with nucleophiles often require complex synthetic strategies.[24] Although coordinated boronic ester systems have been used for cell encapsulation,[25] they have not been applied to tissue differentiation and maturation, nor have they been explored for culturing marbled meat.

In this study, we present a scaffolding technology for cultured meat production using self-healing hydrogels with strong, reversible cross-links under physiological conditions.

https://doi.org/10.1021/acsami.5c03479
ACS Appl. Mater. Interfaces 2025, 17, 31881−31897

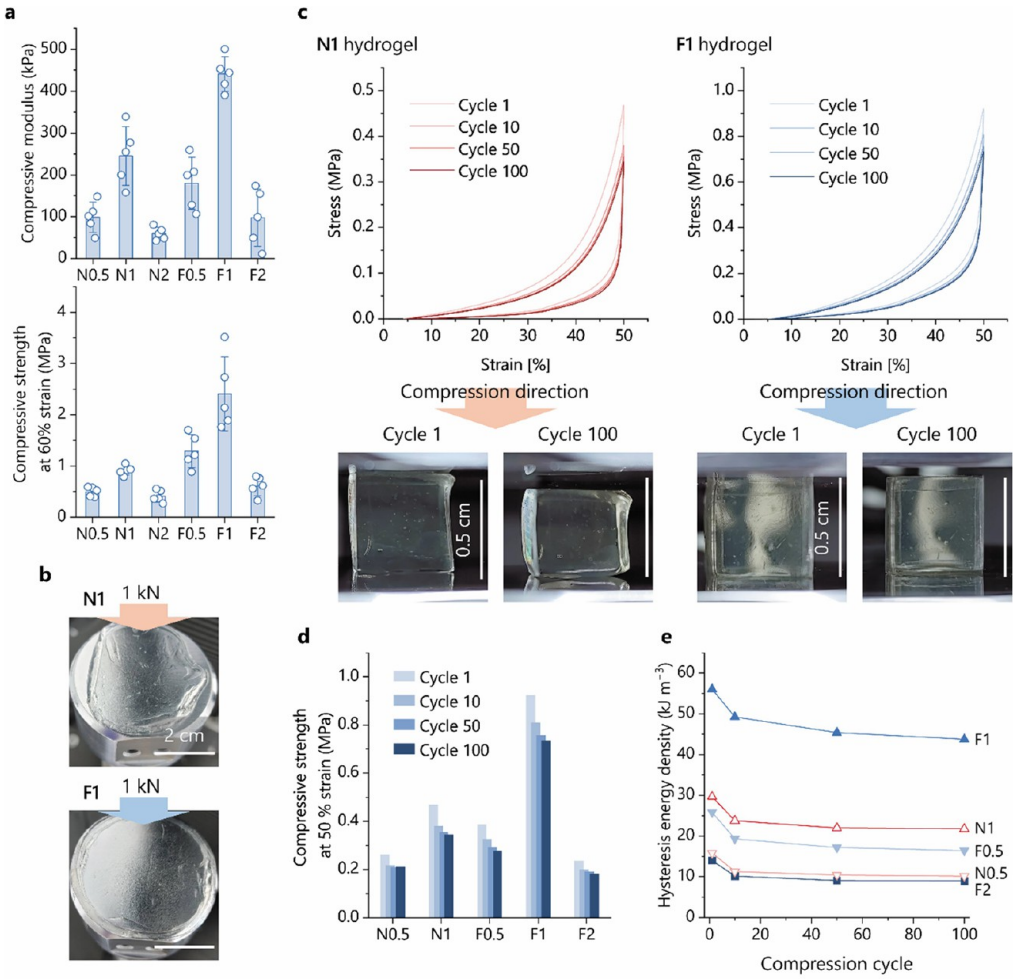

Figure 2. Compressive mechanical properties and hysteresis behavior of $ChsB(OH)_2$/PVA hydrogels. (a) Compressive Young's moduli and strengths at 60% strain. Data are expressed as means ± standard deviations. (b) Representative photos of conventional (**N1**) and freeze−thaw-treated (**F1**) gels after compression at 40 MPa. (c) Compressive loading−unloading curves showing hysteresis loops for the **N1** and **F1** hydrogels at selected cycles, with corresponding photos of the test specimens at the start of the first cycle and the end of the 100th cycle. (d) Compressive strengths at 50% strain and (e) hysteresis energy densities at selected cycles. Data for **N2** are omitted because it failed to sustain the test.

Our strategy relies on an interpenetrating network (IPN) composed of boronic acid-conjugated chitosan [$ChsB(OH)_2$] and poly(vinyl alcohol) (PVA), which features boronic acid−*cis*-diol linkages that enable self-healing, and hydrogen bonds between hydroxy (−OH) and/or amino ($-NH_2$) groups that reinforce the hydrogel. Nanomechanics analysis revealed that the nucleophilic groups of chitosan facilitate boronic acid−diol bond formation, which otherwise requires alkaline conditions, at neutral pH with approximately half the strength of a typical covalent bond. The hydrogel is biocompatible with cell lines and bovine primary cells and exhibits optimized mechano-transduction for monoculturing fat and muscle cells. This scaffolding technology enables the simple assembly of a realistic marbled meat prototype from monocultures without the need for cross-linkers or processing devices (Figure 1) and offers a straightforward method for producing marbled meat in vitro with organoleptic properties and nutritional profiles similar to those of conventional meat.

2. RESULTS AND DISCUSSION

2.1. Self-Healing Hydrogel-Scaffold Design. Boronic acid moieties were introduced into the chitosan backbone by the amide coupling of 3-carboxyphenylboronic acid (3-CPBA) to chitosan (average degree of deacetylation: 0.8) in the presence of carboxyl activators (Scheme S1a). Compared to previously synthesized alginate analogs,[26,27] boronic acid-functionalized chitosan gels at near-physiological pH because the boron center is stabilized by the lone pair of the chitosan nitrogen atom (Scheme S1b).[28] Furthermore, chitosan exhibits antibacterial properties and is biocompatible, making it suitable for meat culturing.[29]

Infrared (IR) spectroscopy confirmed successful grafting, showing characteristic vibrations of *m*-substituted benzene moieties, including aromatic ring stretching (1604 and 1580 cm^{-1}), three-adjacent-C−H out-of-plane deformation (819 and 748 cm^{-1}), and ring C−H out-of-plane bending (705 cm^{-1}) (Figure S1). Proton (^1H) nuclear magnetic resonance (NMR) spectroscopy further verified the coupling, with the 3-CPBA phenyl ring signals appearing at 7.38−8.20 ppm (Figure S2). The degree of boronic-acid conjugation (molar ratio of conjugated amine to total amine) was determined to be 21.2 ± 1.8% by ultraviolet (UV)−visible spectroscopy (Figure S3). Hereafter, we refer to the boronic acid-conjugated chitosan as $ChsB(OH)_2$.

$ChsB(OH)_2$ alone can form boronic ester bonds because chitosan is a diol-containing polysaccharide. An acidic aqueous

https://doi.org/10.1021/acsami.5c03479
ACS Appl. Mater. Interfaces 2025, 17, 31881−31897

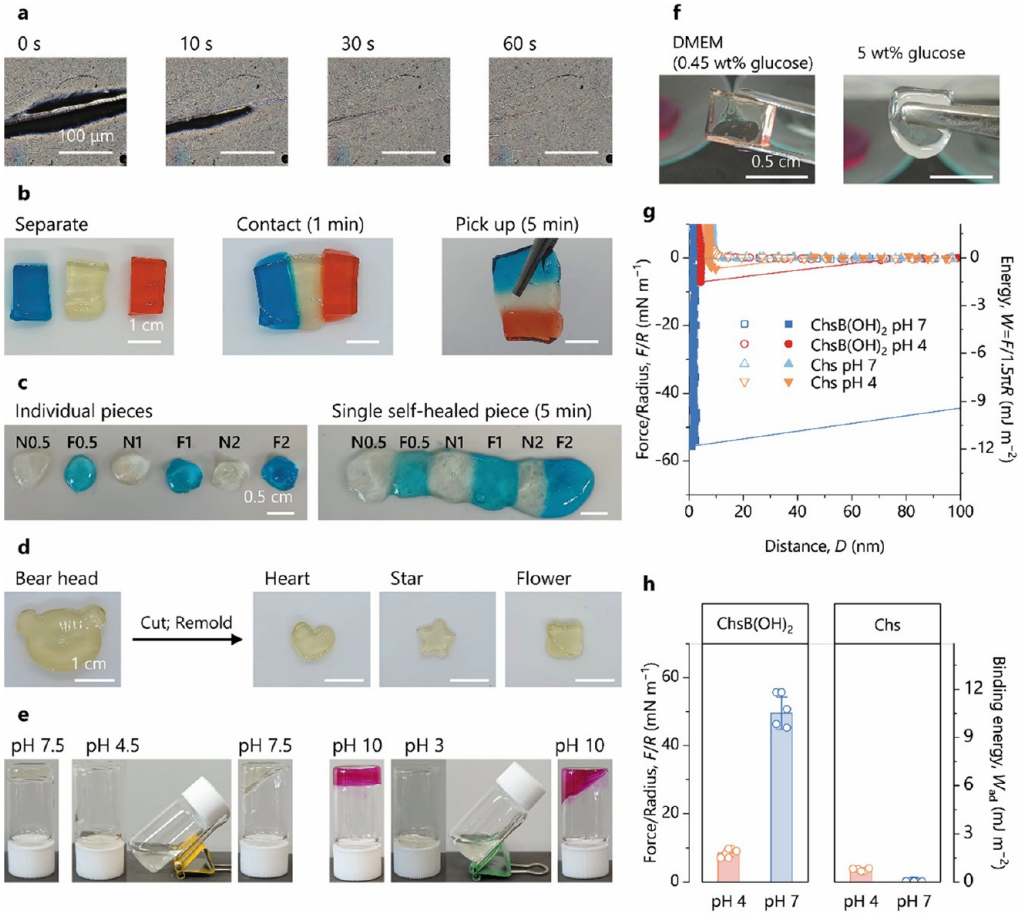

Figure 3. Multifunctionality of $ChsB(OH)_2$/PVA-hydrogel and nanomechanics of boronic acid−diol interactions. (a) Optical microscopic images showing the self-healing process in the **N1** hydrogel observed for the fifth time. The images are captured from Movie S1. Macroscopic fusion of individual pieces of (b) **N1** hydrogel and (c) hydrogels with different compositions. Dyes used: Brilliant Blue FCF and Amaranth Red 2. (d) Reshaping ability of the **N1** hydrogel. (e) pH responsiveness of the **N1** hydrogel, with phenolphthalein as a pH indicator. (f) Responsiveness of the **N1** hydrogel after exposure to Dulbecco's modified Eagle's medium (DMEM) and to a 5 w/v% aqueous glucose solution for 1 min. Surface-force data: (g) force−distance profiles (open symbols represent approaching, and closed symbols represent detaching of the two surfaces) and (h) interaction energies between $ChsB(OH)_2$ and mica, and between chitosan (Chs) and mica surfaces at acidic and neutral pH. Data are expressed as means ± standard deviations.

solution of $ChsB(OH)_2$ (3 wt %) gelled when the pH was increased to 7.4 using 1 M sodium hydroxide (NaOH). This process was driven by boronic ester formation rather than hydrogen bonding between the deprotonated−NH_2 groups (pK_a of 6−6.5), as *N*-conjugation reduced the total amino content of chitosan. Furthermore, the boronic acid moiety prevented aggregation of the chitosan backbone. However, the resulting $ChsB(OH)_2$ hydrogel lacked self-supporting mechanical characteristics, with a compressive modulus of ∼2 kPa (Figure S4). In addition, the rigidity of the chitosan backbone hindered boronic ester formation. These attributes resulted in a hydrogel network that is susceptible to rupture under external forces, posing challenges for tissue culture due to low cell adhesion and dispersal.[30,31]

To enhance the mechanical properties of $ChsB(OH)_2$, we introduced PVA as an external diol source because its flexible backbone facilitates boronic acid−diol bond formation more effectively than $ChsB(OH)_2$ alone. Furthermore, PVA can form hydrogels via repeated freeze−thaw cycles by crystallization through intermolecular hydrogen bonding between −OH groups.[32] $ChsB(OH)_2$/PVA cross-linking produced a hydrogel with an IPN that combined hydrogen bonds and boronic acid−diol ester bonds. Hydrogen bonds provide mechanical reinforcement, whereas boronic acid−diol bonds enable self-healing, both of which are beneficial for 3D cell culturing.[17,33] Hydrogels were prepared by mixing aqueous solutions of $ChsB(OH)_2$ (3 wt %, pH 4) and PVA (10 wt %) at various volume ratios, followed by pH adjustment to 7.4 by dropwise addition of 1 M NaOH. Two types of hydrogels were prepared and denoted as **N***x* and **F***x*, where **N** refers to spontaneously formed hydrogels, **F** refers to hydrogels subjected to a single freeze−thaw cycle, and *x* refers to the $ChsB(OH)_2$-to-PVA volume ratio (Figure S5; Table S1).

Although phenylboronic acids typically have pK_a values of 8−9,[24] all hydrogels were formed within 5 s at physiological pH. This suggests that nitrogen−boron (N→B) coordination stabilizes the boronic acid−diol ester linkage.[28] The ester bond formation was confirmed by the appearance of the B−OR asymmetric vibration at 1235 cm^{-1} in the IR spectra of the hydrogels. This signal was absent in $ChsB(OH)_2$ and the $ChsB(OH)_2$/PVA mixture at pH 4, where the chitosan amino groups were protonated, preventing N→B coordination (Figure S6a).[34] Strong $ChsB(OH)_2$−PVA interactions were further supported by a high gel fraction[35] (>60%) observed for all the samples (except **N2**), indicating high cross-linking densities (Figure S7).

https://doi.org/10.1021/acsami.5c03479
ACS Appl. Mater. Interfaces 2025, 17, 31881−31897

Freeze−thaw treatment induced additional PVA cross-linking via hydrogen bonding, as evidenced by the **F** series exhibiting higher gel fractions than those of the **N** series. The IR spectra revealed the broadening and redshift of the O−H stretching signal from 3309 to 3288 cm^{-1} in the **N** series to 3282−3279 cm^{-1} in the **F** series (Figure S6b), which is consistent with increased hydrogen bonding.[36] Hydrogels with equal $ChsB(OH)_2$-to-PVA volumes (**N1** and **F1**) exhibited the highest gel fractions. Conversely, lower $ChsB(OH)_2$ contents (**N0.5** and **F0.5**) resulted in insufficient boronic acid concentrations, whereas higher $ChsB(OH)_2$ contents (**N2** and **F2**) led to lower chain mobility, both of which reduced effective cross-linking (Figure S7). Scanning electron microscopy (SEM) and swelling experiments corroborated these observations; samples with higher gel fractions exhibited smaller pores and lower swelling degrees, and vice versa (Figure S8).

2.2. Strong, Rapidly Self-Healing, Multi-Modularly Responsive Hydrogels. Microenvironmental mechanical signals significantly influence cell spreading, migration, and differentiation via mechanotransduction.[15] Therefore, hydrogels with tailored mechanical properties are desirable because different stiffnesses are required for the proliferation and differentiation of distinct cell types, such as fat and muscle cells.[37]

The mechanical properties of the prepared hydrogels were assessed using compression testing (Figure 2). The hydrogels exhibited compressive Young's moduli of 59.6−440 kPa and compressive strengths of 0.41−2.41 MPa at 60% strain (Figures 2a and S9). Within the **N** series, the **N1** hydrogel displayed the highest mechanical performance owing to an optimal balance between the boronic acid−diol interactions and chain mobility. The large stiffness window allows the selection of scaffolds suitable for different tissue types that exhibit substantial stiffness variation (2.5−3 kPa for fat and 3−800 kPa for muscle).[38]

Cell-laden materials must withstand repeated expansion and compression as cells grow and proliferate.[39] The $ChsB(OH)_2$/PVA hydrogels effectively dissipated stress and self-healed microcracks. Both **N** and **F** hydrogels showed no visible surface or interior damage after compression at 40 MPa (Figures 2b and S9). Additionally, the hydrogels were subjected to 100 successive compressive loading−unloading cycles at 50% strain with 10 s relaxation intervals, with all **N** and **F** hydrogels retaining their energy dissipation capabilities (Figures 2c and S10). **N1** and **F1** exhibited hysteresis loops after 100 cycles that were not noticeably different from those recorded after the first cycle, with only a slight reduction in height (∼10%) (Figure 2c). All **N** and **F** hydrogels retained >71% of their compressive strengths and 63.4−78.0% of their hysteresis energy densities following testing (Figure 2d,e). Furthermore, they dissipated more than 55.6% of the loaded stress (Figure S11). These excellent recovery and fatigue resistance properties are attributable to dynamic boronic ester rearrangement, sacrificial hydrogen bonds, and friction between polymer chains.[19,27,40] These properties are valuable for in vitro meat culturing, which requires weeks for the cells to mature into tissue-like structures.

Dynamic boronic ester bond rearrangement at the molecular level endowed the **N** and **F** hydrogels with self-healing and reshaping capabilities.[27] Optical microscopy showed the progressive self-healing process of the **N1** hydrogel, which fully repaired a ∼0.2 mm scratch within 4−5 min, a process that was repeatable at least five times (Figure 3a; Movie S1).

A typical trade-off exists between stiffness and self-healing because high segmental motion oppositely affects these properties.[41] However, the self-healing abilities of the **F** hydrogels were not significantly impeded, implying that PVA crystallization minimally affected the boronic ester bond. The stiffer **F1** hydrogel required up to 15 min to fully heal, while the softer **N0.5** hydrogel healed within 2 min. Self-healing manifests through efficient interfacial fusion between individual hydrogels with identical or different chemical compositions and mechanical properties (Figure 3b,c), which offers significant advantages for assembling muscle and fat tissues grown on scaffolds with different stiffness. Furthermore, reshaping ability was observed: a large **N1** hydrogel piece was molded into a shape resembling a teddy bear's head and subsequently cut and morphed into smaller shapes (star, flower, and heart) without external treatment (Figure 3d).

Boronic acid−*cis*-diol molecular dynamics also endowed the $ChsB(OH)_2$/PVA hydrogels with macroscopic pH responsiveness. The **N1** hydrogel, initially formed at pH 7.5, collapsed at pH 4.5 due to boronic acid−*cis*-diol bond dissociation and chitosan amino group protonation, which further destabilized the boron center. A stable gel was immediately reformed when the pH increased to 7.5, and this behavior was observed over a broad pH range of 3−10 (Figure 3e). This pH responsiveness was further quantified via rotational rheometry in the 0.1−10 Hz range (Figure S12a). At pH 7.5, the storage modulus (G') of **N1** was higher than its loss modulus (G'') across the examined frequency range, whereas at pH 4.5, G' was lower than G''. At pH 6.5, which corresponds to the pK_a of chitosan amino groups, G' was lower than G'' at frequencies below 1 Hz but higher than G'' at frequencies above 1 Hz, indicating partial N→B coordination.

The pH-dependent nanomechanics of the boronic ester bond at the molecular level was investigated using a surface forces apparatus (SFA). One mica surface was coated with $ChsB(OH)_2$ or chitosan, whereas the opposite surface remained uncoated since muscovite mica is inherently rich in hydroxy groups.[42] Adhesion forces were measured as a function of the mica−mica distance (D). The two surfaces were contacted at the steric wall distance (D_{SW}), which remained relatively constant with increasing compressive force (Figure S13).

An attractive force (F/R) of 49.5 mN m^{-1} (absolute value), corresponding to a binding (adhesion) energy (W) of 10.5 mJ m^{-2}, was measured for the boronic acid−diol interaction after only 30 s of contact at pH 7. This rapid binding confirms that molecular N→B coordination stabilized the boronic acid−diol complexation under (near-)neutral conditions. Significantly (5.8-times) lower F/R and W values were recorded at pH 4 (8.56 mN m^{-1} and 1.82 mJ m^{-2}, respectively) (Figure 3g,h). This was attributed to the protonation of chitosan amino groups, resulting in the breakage of the N→B coordination and the release of free boronic acid, which destabilizes the boronic acid−diol interaction.

In contrast, chitosan exhibited minimal interactions with the mica surface within 30 s at both acidic and neutral pH (W values of 0.79 and 0.06 mJ m^{-2}, respectively). Although chitosan is expected to adhere to mica through electrostatic attraction at pH 4 and hydrogen bonding at pH 7, their directionality was insufficiently optimized over a short contact period.[43,44] This observation is consistent with the rapid

https://doi.org/10.1021/acsami.5c03479
ACS Appl. Mater. Interfaces 2025, 17, 31881−31897

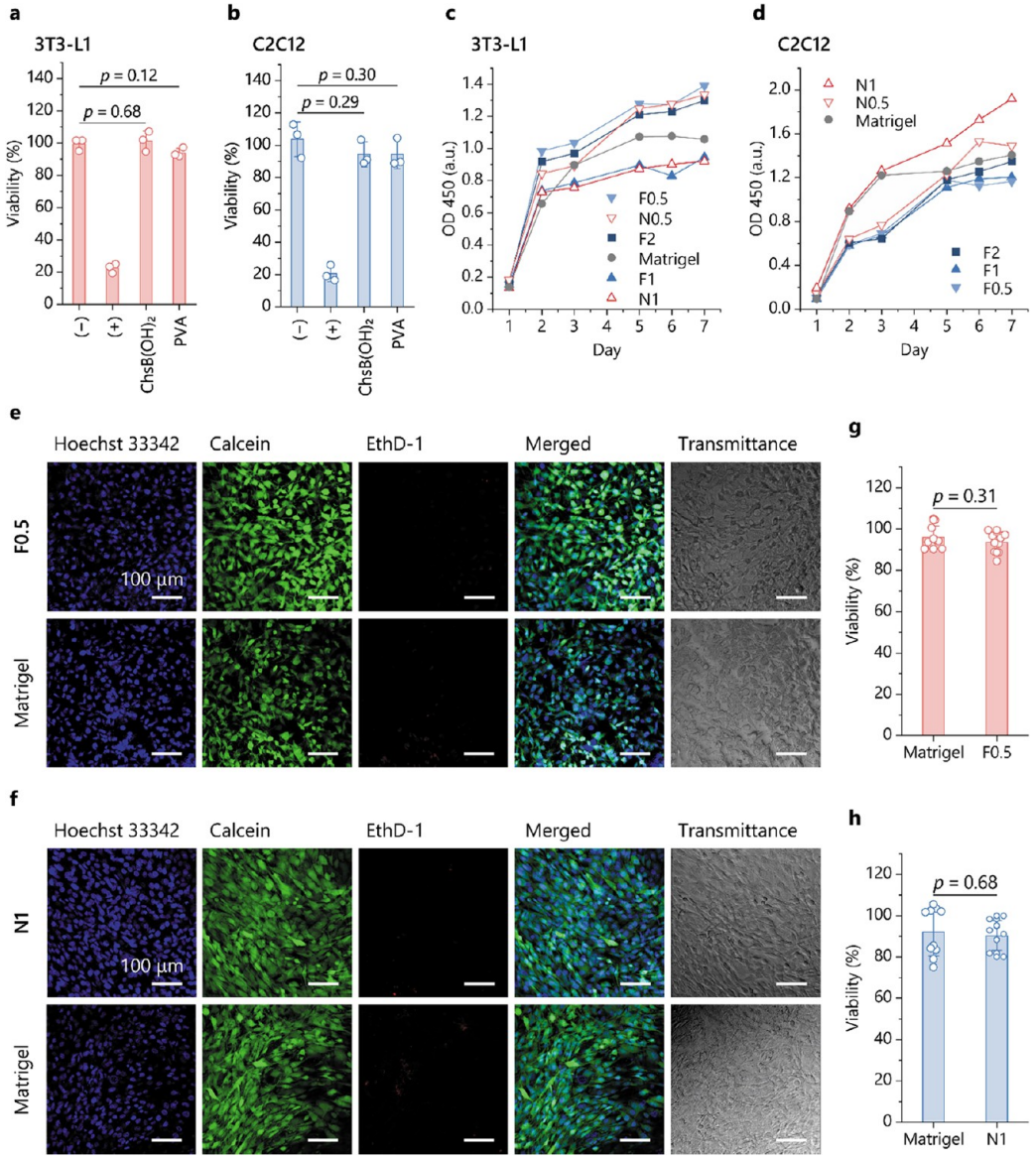

Figure 4. Biocompatibility and proliferation of preadipocyte 3T3-L1 and muscle C2C12 cells in ChsB(OH)$_2$/PVA hydrogels. Cytotoxicity of hydrogel components toward (a) 3T3-L1 and (b) C2C12 cells using the water-soluble tetrazolium (WST-8) assay following the ISO 190993 standard. Low-density polyethylene and zinc diethyldithiocarbamate were used as the negative and positive controls, respectively. (c) 3T3-L1 and (d) C2C12 proliferation in ChsB(OH)$_2$/PVA hydrogel scaffolds, determined by monitoring the absorbance of formazan dye at 450 nm, reduced from WST-8 by viable cells. Confocal images showing the morphologies of predifferentiated (e) 3T3-L1 and (f) C2C12 cells cultured for 3 d in **F0.5** and **N1** hydrogels, respectively, compared to Matrigel (positive control). Viable cells were stained with calcein (green), dead cells with ethidium homodimer-1 (EthD-1, red), and nuclei with Hoechst 33342 (blue). Viability of (g) 3T3-L1 and (h) C2C12 cells in ChsB(OH)$_2$/PVA hydrogels relative to Matrigel, determined from the fluorescence intensity at 530 nm of calcein-dyed cells. Data are expressed as means ± standard deviations; *p* values were calculated using two-tailed Student's *t*-tests.

formation of ChsB(OH)$_2$/PVA hydrogels upon pH adjustment from 4 to 7.5 (Section 2.1), confirming that the boronic acid–diol ester bonding surpassed the hydrogen bonding responsible for chitosan aggregation.

These results highlight the dynamic covalent nature of boronic acid–diol interactions in aqueous environments. Its binding energy overlaps the higher range of many noncovalent interaction motifs that have been exploited for underwater adhesion applications,[45] while being weaker than a C–C covalent bond, which typically has an SFA-determined W value of 50 mJ m^{-2}.[46] This strong, dynamic bond is beneficial for cell-laden hydrogels, as it provides integrity while facilitating stimulus-responsive control of the cellular microenvironment.[17,47]

One major concern of using ChsB(OH)$_2$/PVA hydrogels in cell culture is the potential interference from glucose in the culture medium because saccharides can compete with PVA for binding to ChsB(OH)$_2$.[26,27] However, the **N1** hydrogel remained stable in Dulbecco's modified Eagle's medium (DMEM) containing 0.45 w/v% glucose (Figure 3f; Movie S2), as evidenced by a G' value comparable to that of virgin **N1** (Figure S12b). In contrast, the hydrogel quickly transformed into a free-flowing liquid when exposed to a 5 w/v% aqueous glucose solution because the strong boronic acid–glucose interaction progressively disintegrated the ChsB-

https://doi.org/10.1021/acsami.5c03479
ACS Appl. Mater. Interfaces 2025, 17, 31881−31897

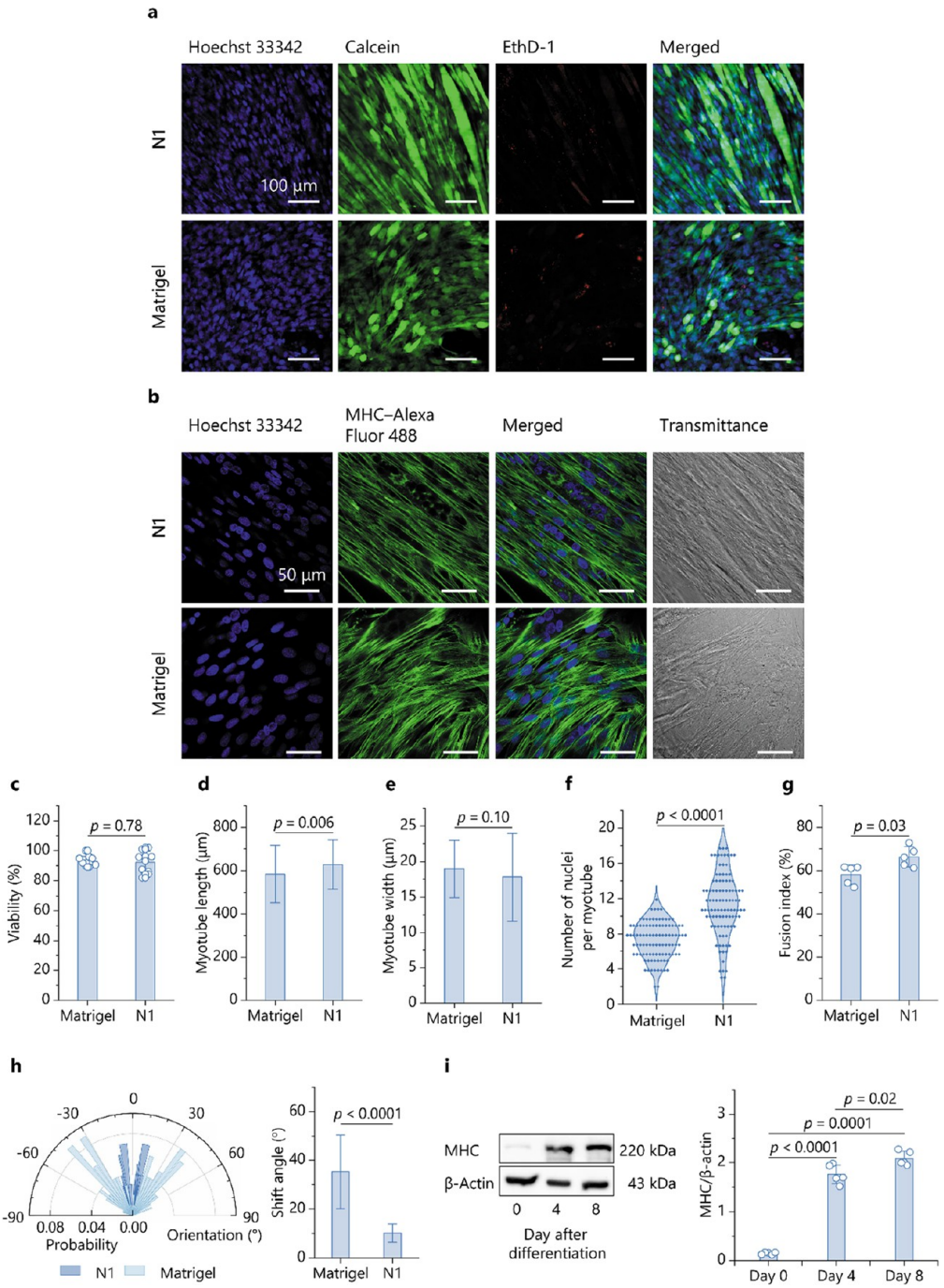

Figure 5. Myogenic differentiation of C2C12 in the **N1** hydrogel compared to Matrigel (positive control). (a) Confocal images of 9-d-differentiated C2C12 cells. Viable cells were stained with calcein (green), and dead cells with ethidium homodimer-1 (EthD-1, red). (b) Confocal images showing the morphologies and immunofluorescence of 9-d-old myotubes stained with Alexa Fluor 488 (green)-conjugated antibodies against myosin heavy chain (MHC); nuclei were counterstained with Hoechst 33342 (blue). (c) Viability of 9-d-old myotubes determined from the fluorescence intensity at 530 nm of calcein-dyed cells. Analyses of C2C12 myogenic differentiation from confocal images, including measurements of myotube (d) lengths, (e) widths, (f) nuclei-per-myotube distribution, (g) fusion index, and (h) myotube-orientation distribution and average shift angles. (i) Western blot quantifying MHC expression relative to β-actin in C2C12 cells lysed at 0 (predifferentiation), 4, and 8 d after differentiation in the **N1** hydrogel. Each lane was loaded with 15 μg of protein. The corresponding uncropped western blot image is shown in Figure S15. Data are expressed as means ± standard deviations. Data for (d–f) and (h) were obtained using 100 random myotubes from three independent experiments; p values were calculated using two-tailed Student's t-tests.

$(OH)_2$–PVA cross-linking. This transformation was accompanied by a nearly 60-fold decrease in G'.

2.3. Culturing Marbled Meat Using Self-Healing Hydrogel Scaffolds. To provide a proof-of-concept for the use of self-healing ChsB$(OH)_2$/PVA hydrogels to construct marbled cultured meat, we grew and matured 3T3-L1 (a preadipocyte fibroblast cell line from mouse embryos) and C2C12 (a muscle myoblast cell line from mice) cells on hydrogel scaffolds. First, we assessed the biocompatibility of the hydrogel components using the water-soluble tetrazolium

https://doi.org/10.1021/acsami.5c03479
ACS Appl. Mater. Interfaces 2025, 17, 31881–31897

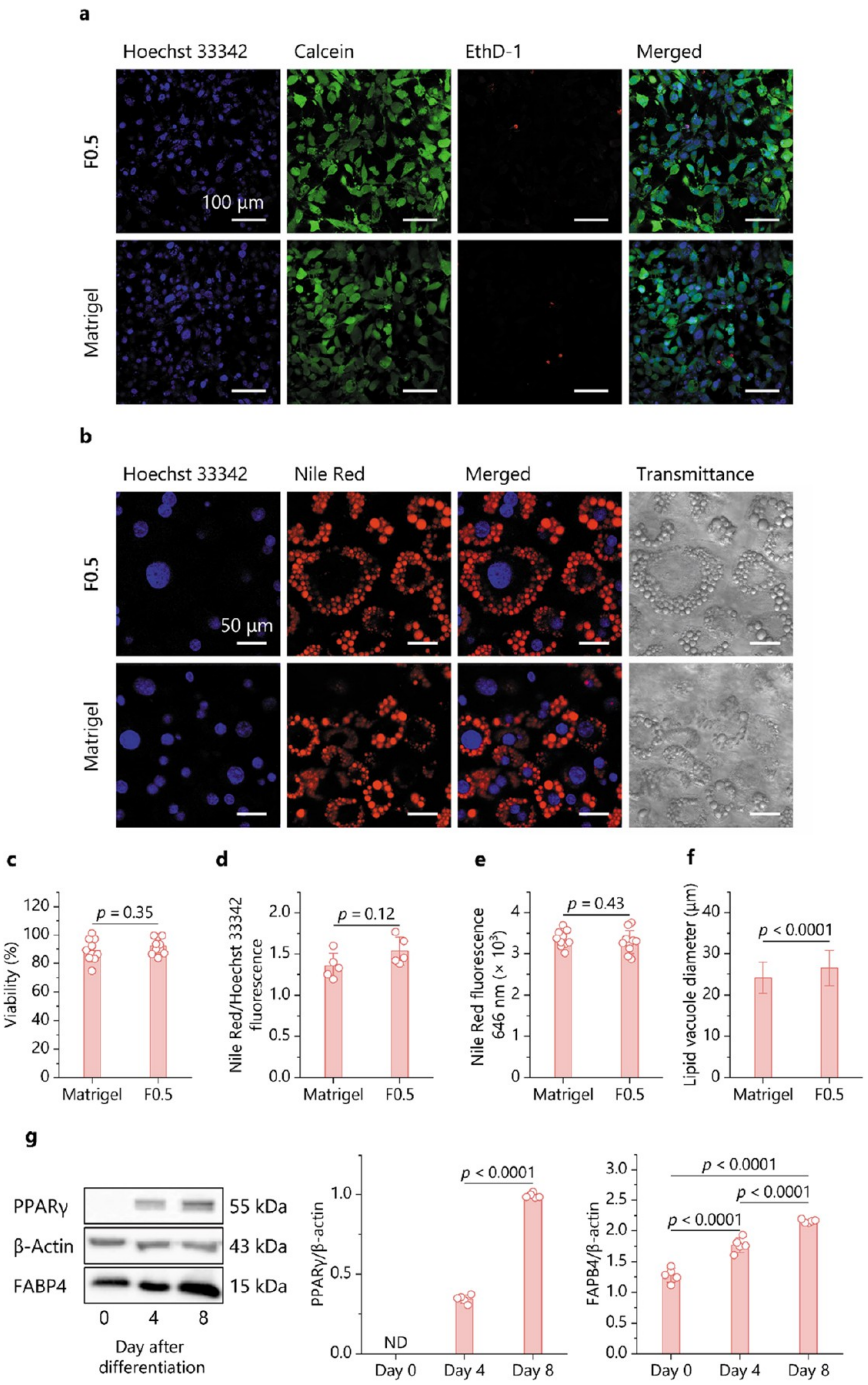

Figure 6. Adipogenic differentiation of 3T3-L1 in the **F0.5** hydrogel compared to Matrigel (positive control). (a) Confocal images of 9-d-differentiated 3T3-L1 cells. Viable cells were stained with calcein (green), and dead cells with ethidium homodimer-1 (EthD-1, red). (b) Confocal images showing the morphology and fluorescence of 9-d-old adipocytes. Lipid droplets were stained with Nile Red (red), and nuclei with Hoechst 33342 (blue). (c) Viability of 9-d-old adipocytes determined from the fluorescence intensity at 530 nm of calcein-dyed cells. (d) Lipid production per cell determined from the ratio of red-to-blue signal areas in the confocal images. (e) Total lipid production of 9-d-old adipocytes determined from the fluorescence intensity at 646 nm of Nile-Red-dyed cells. (f) Average diameters of lipid droplets (n = 100) obtained from five random confocal images across three independent experiments. (g) Western blot quantifying the expressions of peroxisome proliferator-activated receptor gamma (PPAR-γ) and fatty acid binding protein 4 (FABP4) relative to β-actin in 3T3-L1 cells lysed at 0 (predifferentiated), 4 and 8 d after differentiation in the **F0.5** hydrogel; ND, not detected. Each lane was loaded with 15 μg of protein. The corresponding uncropped western blot image is shown in Figure S16. Data are expressed as means ± standard deviations; p values were calculated using two-tailed Student's t-tests.

(WST-8)-based assay (commercially available as Cell Counting Kit-8; CCK-8).[48] Both hydrogel precursors exhibited no observable cytotoxicity toward either cell type, with viabilities exceeding 70%, which complied with the ISO 10993-5 standard (Figure 4a,b). We subsequently evaluated cell proliferation in hydrogel scaffolds with varying compressive stiffness over 1 week using the CCK-8 assay and compared the results with those for cells cultured in Matrigel (an ECM mimic) as a positive control (Figure 4c,d).[49] These comparisons helped select the scaffold with the compressive

https://doi.org/10.1021/acsami.5c03479
ACS Appl. Mater. Interfaces 2025, 17, 31881−31897

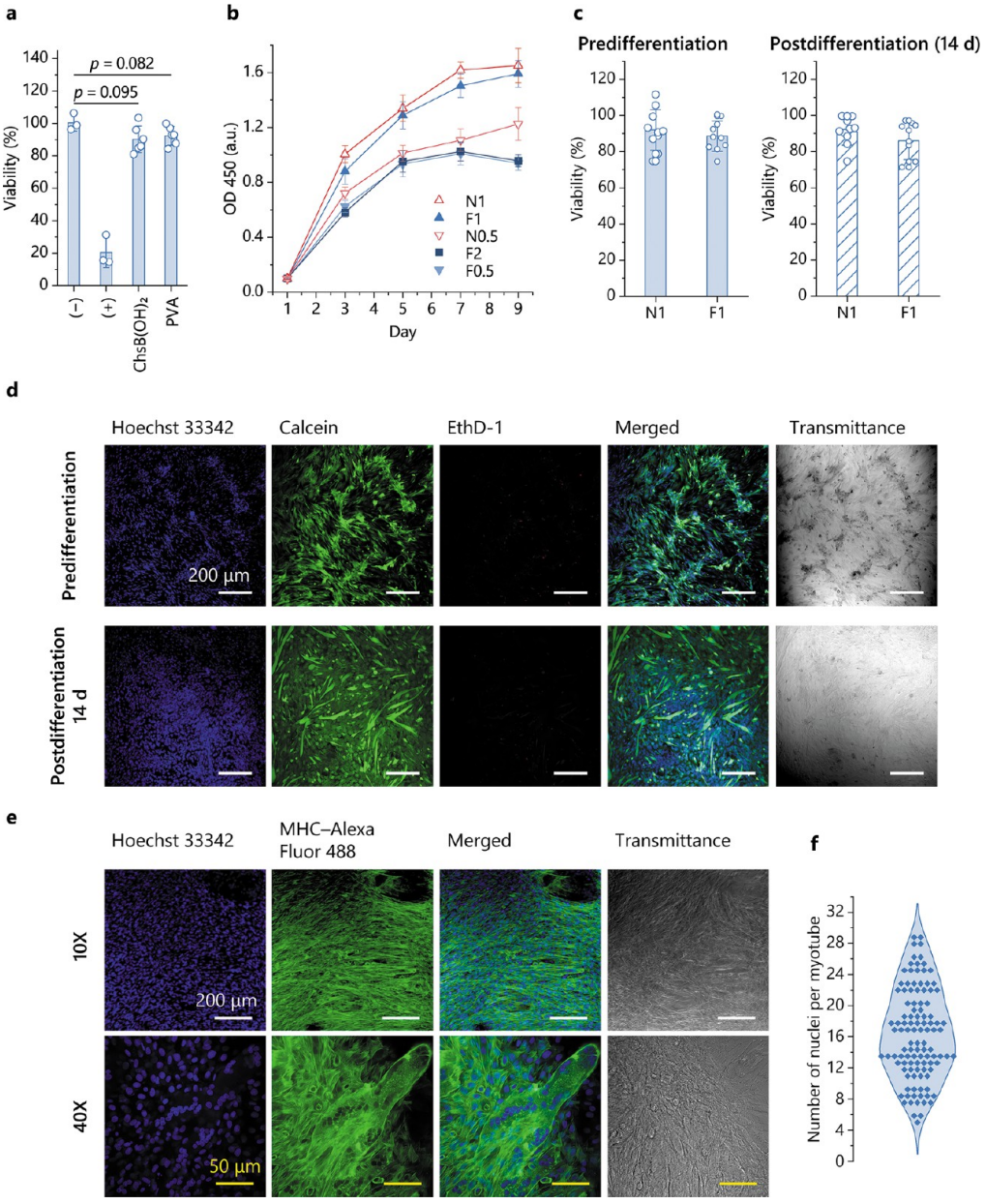

Figure 7. Proliferation and differentiation of Hanwoo primary muscle cells (bMuSC) in $ChsB(OH)_2$/PVA hydrogel scaffolds. (a) Cytotoxicity of hydrogel components toward the cells using the water-soluble tetrazolium (WST-8) assay following the ISO 190993 standard. Low-density polyethylene and zinc diethyldithiocarbamate were used as the negative and positive controls, respectively. (b) Cell proliferation in hydrogels with varying compressive moduli, determined by monitoring the absorbance of formazan dye at 450 nm, reduced from WST-8 by viable cells. (c) Viability of 5-d-old predifferentiated cells and 14-d-old differentiated cells in **N1** and **F1** hydrogels, determined from the fluorescence intensity at 530 nm of calcein-dyed cells. (d) Confocal images showing the morphologies of predifferentiated cells (upper panels) and 14-d-old differentiated myotubes (lower panels). Viable cells were stained with calcein (green), and dead cells with ethidium homodimer-1 (EthD-1, red). (e) Confocal images showing the morphologies and immunofluorescence of 14-d-old myotubes stained with Alexa Fluor 488 (green)-conjugated antibodies against myosin heavy chain (MHC); nuclei were counterstained with Hoechst 33342 (blue). (f) Analysis of bMuSC myogenic differentiation from confocal images, showing the distribution of nuclei per myotube. Data are expressed as means ± standard deviations; *p* values were calculated using two-tailed Student's *t*-tests.

stiffness most compatible with each cell type for further experiments. Overall, all hydrogel scaffolds supported cellular growth, with the proliferation rates varying with the cell type. Softer hydrogels (**F0.5**, **N0.5**, and **F2**) promoted 3T3-L1 cell growth, whereas C2C12 cells proliferated more effectively in the stiffer **N1** hydrogel.

The viabilities of C2C12 and 3T3-L1 cells cultured on **N1** and **F0.5** scaffolds, respectively, were visualized using LIVE/DEAD imaging. Confocal microscopy of hydrogel cross sections revealed that cells initially seeded on the surface migrated into the interior and displayed typical fibroblast and myoblast morphologies after 3 d (Figure 4e,f). Quantification of viable cells via calcein fluorescence showed over 90% viability, which was comparable to that of Matrigel (Figure 4g,h).

In rigidly cross-linked hydrogels, cells typically retract, assume round morphologies, and fail to interact effectively.[50,51] This necessitates a high seeding density (e.g., up to 8×10^6

https://doi.org/10.1021/acsami.5c03479
ACS Appl. Mater. Interfaces 2025, 17, 31881−31897

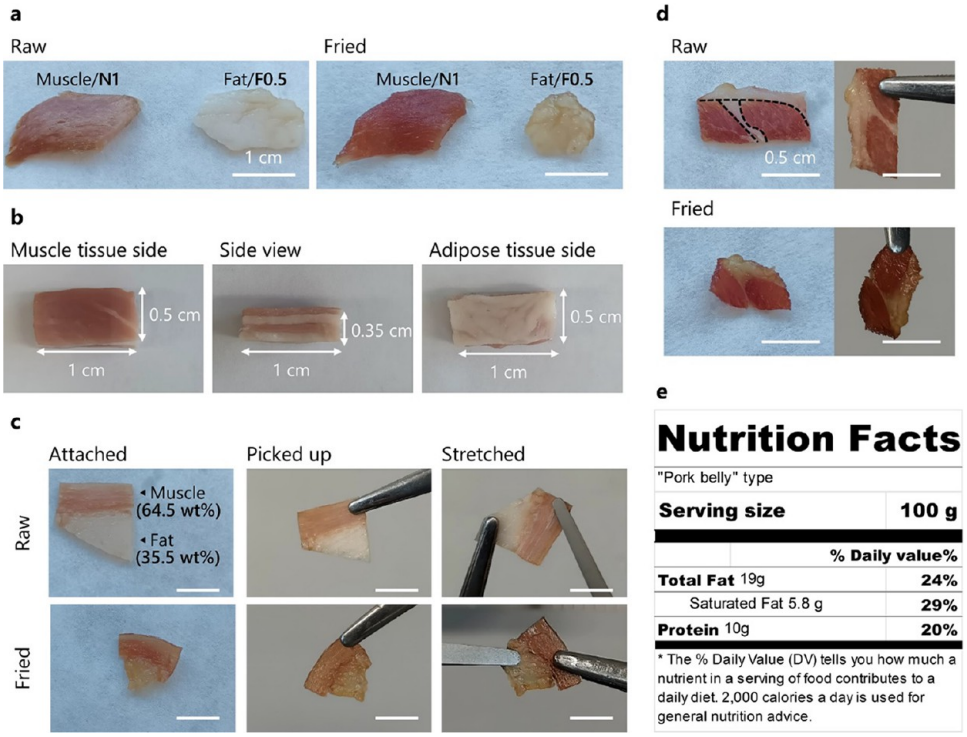

Figure 8. Differently assembled cultured meat prototypes. (a) Individual cultures of 28-d-old muscle and fat tissue before and after frying. (b) Meat prototype constructed by alternately stacking muscle and adipose tissue to form two adhesive bilayers. (c) Meat prototype fabricated by joining fat and muscle cultures in an edge-to-edge manner. Fat−muscle interfacial adhesion enabled the meat to be picked up and stretched. The adhesion remained after frying and only broke under strong stretching (Movie S3). (d) Complex marbled structure of natural red meat mimicked in a meat prototype constructed using four individual tissue cultures (two fat and two muscle), with borders indicated with dashed lines. Muscle tissue was stained with carmine (red), while fat tissue remained unstained. The meat was fried in sunflower oil at 150 °C for 4 min. (e) Nutritional composition of the meat prototype shown in (c), with %daily values calculated based on the US Food & Drug Administration's recommended guidelines.[59]

cells mL^{-1}) to facilitate cellular interaction, leading to tissue-culturing cost burden.[52] In contrast, the dynamic boronic acid−diol ester cross-links in the $ChsB(OH)_2$/PVA hydrogels enabled the cells to spread and form an interconnected network, promoting effective interaction, differentiation, and desired tissue formation. Even at a low seeding density (5×10^4 cells per well, 24-well plate), the cells proliferated effectively (Figure S14). Furthermore, scaffold dynamicity allowed for effective 3D cell culture via seeding, thereby overcoming the viscosity challenges associated with precursor-based cell encapsulation.

The myogenic differentiation of C2C12 cells was evaluated through myotube formation and myosin heavy chain (MHC) expression.[53] After 9 d of differentiation, C2C12 cells in the **N1** hydrogel fused to form elongated, multinucleated myofibers with high cellular viability, comparable to those in Matrigel (>95%; Figure 5a−c). Although the myotubes in both scaffolds exhibited similar lengths and widths (Figure 5d,e), thoses in the **N1** hydrogel showed a higher number of nuclei per myotube and a greater fusion index (ratio of nuclei within myotubes to total nuclei) than those in Matrigel (Figure 5f,g). Interestingly, despite the absence of topographic cues, the myotubes in the **N1** hydrogel were more aligned, with an average angle shift of 10.2° compared to 35.3° in Matrigel (Figure 5h). Since myoblast fusion and myotube alignment are sequential events during muscle maturation,[54] these results suggest that the **N1** hydrogel effectively supported C2C12 myogenic differentiation. This was further confirmed by western-blot analysis, which showed significant increases in MHC expression, with levels 1.76- and 2.08-times that of β-actin, a housekeeping protein, at days four and eight of myogenic differentiation, respectively (Figure 5i).

Adipogenesis of 3T3-L1 fibroblasts was evaluated by monitoring lipid formation. After 9 d of differentiation, lipid droplets accumulated in cells cultured in both **F0.5** and Matrigel, appeared as vacuoles in LIVE/DEAD-stained images (Figure 6a), and stained red with Nile Red, in contrast to Hoechst 33342-stained nuclei (blue) (Figure 6b). Both scaffolds exhibited adipocyte viabilities exceeding 90% (Figure 6c). Lipogenesis per cell, quantified by comparing the Nile Red fluorescence to that of Hoechst 33342, revealed similar ratios in adipocytes grown in the **F0.5** scaffold and Matrigel (1.53 and 1.35, respectively) (Figure 6d), consistent with the total lipid production measurements based on the Nile Red fluorescence intensity (Figure 6e). Morphologically, the lipid droplets in the **F0.5** scaffold had a slightly larger maximum width (26.5 μm) than those in Matrigel (24.1 μm) (Figure 6f). At the protein level, adipogenesis was confirmed by comparing the expression of peroxisome proliferator-activated receptor gamma (PPAR-γ), a crucial regulator of adipogenesis, and fatty acid-binding protein 4 (FABP4), a carrier protein for fatty acids in mature adipocytes, to that of β-actin.[55] Western blotting revealed that differentiated adipocytes upregulated the expressions of PPAR-γ (0.31-times at day four and 0.98-times at day eight postdifferentiation) and FABP4 (1.77-times at day four and 2.16-times at day eight postdifferentiation) compared to undifferentiated 3T3-L1 cells (Figure 6g). These findings

https://doi.org/10.1021/acsami.5c03479
ACS Appl. Mater. Interfaces 2025, 17, 31881−31897

suggest that the soft **F0.5** scaffold effectively supported 3T3-L1 adipogenesis.

Owing to their well-defined characteristics, cell lines are increasingly used for the research and development of cultured meat. Some companies are attempting to commercialize meat derived from immortalized cell lines. However, most still depend on primary cells for commercial meat production due to regulatory hurdles.[56] Therefore, we explored the potential of self-healing hydrogels to cultivate and differentiate bovine primary muscle cells (bMuSC) sourced from Hanwoo cattle.

All hydrogel components were biocompatible with bMuSC cells, with cell viability exceeding 70%, as measured by the WST-8 assay (Figure 7a). The stiff **N1** and **F1** hydrogels promoted the fastest bMuSC proliferation (Figure 7b), similar to the results observed in C2C12 cells, suggesting that muscle cells respond similarly to stiff hydrogels via mechanotransduction. LIVE/DEAD confocal imaging revealed that the bMuSC cells adopted spindle-like morphologies after 5 d of predifferentiation culture. After 14 d of differentiation, myotube formation was evident, characterized by elongated cytoplasmic structures (Figure 7d). Calcein fluorescence quantification showed that approximately 90% of both predifferentiated and differentiated cells were viable in the **N1** and **F1** hydrogels (Figure 7c). MHC immunostaining of differentiated Hanwoo muscle cells revealed a network of elongated structures containing multiple nuclei within a single membrane, which is characteristic of myotubes (Figure 7e). On average, the myotubes were 23.5 ± 4.37 μm wide, had a fusion index of 78.5 ± 6.58%, and contained a median of 13 nuclei per myotube (Figure 7f).

These results demonstrated that our self-healing scaffolding technology effectively supported the growth and differentiation of both cell lines and primary cells. Although mature whole-muscle beef production remains forthcoming, the structural control, mechanical strength, and adhesion capability achieved in the mouse meat prototype (discussed below) suggest that this self-healing hydrogel can facilitate the development of marbled cultured beef with desired organoleptic properties.

We constructed a marbled cultured meat prototype by assembling **N1** and **F0.5** scaffolds that were growing 28-d-old 3T3-L1 adipocytes and C2C12 muscle-like cells, respectively. To distinguish cell types, muscle cells were stained red with carmine, a common food coloring used in processed meat, rendering fat cells white.[14] Monocultures of muscle and fat tissues up to 1.5 cm × 1 cm × 0.1 cm in size were produced (Figure 8a). The remarkable self-healing ability of the scaffolds enabled robust muscle−fat adhesion. Furthermore, their ratios and patterns within the prototype could be customized, including sandwiched (Figure 8b) and edge-to-edge fused (Figure 8c) muscle−fat layers, resembling the structure of pork belly, and the intricate marbling found in steak (Figure 8d). Larger pieces could also be assembled from smaller individual cultures, eliminating the need to coculture large tissue blocks, which often leads to cell death due to insufficient nutrient and oxygen supply to the tissue core.[57] Notably, the muscle−fat interfaces formed without cross-linkers exhibited strong adhesion that was not easily broken under significant stretching (Movie S3).

The prepared meat prototype was then fried to assess its cooking potential. The texture of the cooked meat resembled that of bacon, a type of processed meat lacking vascular tissue, and the muscle−fat interface remained intact after frying (Figure 8c, Movie S3). We anticipate that introducing vascular cells into this meat prototype through self-healing will further impart its textural resemblance to marbled beef.

The nutritional composition of the pork belly like meat prototype, formed by edge-to-edge adhesion of the muscle (64.5 wt %) and fat (35.5 wt %) blocks, was analyzed (Figure 8e; Table S2). This prototype contained two key macronutrients found in meat: protein (10 wt %) and fat (19 wt %), with unsaturated fats comprising 69.5 wt % of the total fat content, a proportion within the typical unsaturated fat range (60−70%) found in conventional meat.[58] Compared to previous attempts at producing marbled meat,[10,14] self-healing scaffolding technology provides optimal conditions for the differentiation and maturation of muscle and fat, thus enabling the fabrication of more realistic meat with tailored organoleptic properties through simple yet precise modulation of both texture and nutritional composition.

We then evaluated the elemental composition of the meat prototype. After differentiation for 28 d, the elemental compositions of the cultures (including the scaffold and tissue) were significantly different from those of their respective hydrogels (Table S3). The 3T3-L1/**F0.5** culture exhibited a higher carbon content as adipocytes accumulated long-chain triglycerides, which was consistent with the lipid content analysis (Table S2). The C2C12/**N1** culture exhibited higher nitrogen and oxygen contents, likely attributable to the muscle proteins. The elemental compositions of the differentiated C2C12 and 3T3-L1 cells closely matched the database values for muscle and fat cells, respectively (Table S4), suggesting that the dynamic scaffolds supported the regular development of muscle and fat.

The safety of the meat prototype was also addressed. The hydrogel components (chitosan and PVA) are generally regarded as safe for use in foods and drugs.[60,61] Boric acid/borax (H_3BO_3/BO_3^{3-}) can be used as a food additive at concentrations up to 0.4 wt %,[62] whereas organoboron (C−B containing) compounds and their derivatives/conjugates are notably less cytotoxic than boric acid and have been widely used in therapeutic applications.[63−65] Boron is a trace element naturally present in many foods, especially plant-based, and is beneficial for certain biological functions.[66]

We assessed the boron content of the 28-d cultures, which was less than 0.07 wt % (corresponding to a boric acid equivalent of <0.4 wt %) (Table S5). To further reduce the boron content, we leveraged the glucose responsiveness of $ChsB(OH)_2$/PVA hydrogels and attempted to disintegrate the scaffold by soaking the muscle/fat assembly in a 5 wt % glucose solution for 1−3 h. The fat/muscle interface remained virtually intact with only 12.1 wt % loss (Figure S17a), and the boric acid equivalent decreased from 0.33 to 0.28 wt % (Figure S17b), indicating that a small fraction of the hydrogel was removed from the meat product. The final boric acid equivalent remained within safe limits. In addition, boron is conjugated to chitosan via an amide linkage, which is not readily hydrolyzed enzymatically in the human body, suggesting minimal physiological effects. Although these findings are promising, more vigorous in vitro and in vivo studies are required to assess the toxicological risks of long-term cultured meat consumption and establish regulations for food safety.

3. CONCLUSIONS

We developed a self-healing scaffolding technology for marbled meat cultivation. The scaffolds consist of chitosan conjugated

https://doi.org/10.1021/acsami.5c03479
ACS Appl. Mater. Interfaces 2025, 17, 31881−31897

to boronic acid [ChsB(OH)$_2$] and poly(vinyl alcohol) (PVA), which form an interpenetrating network of dynamic boronic acid−*cis*-diol esters and hydrogen bonds. This material rapidly self-healed and reshaped under physiological conditions, and was responsive to various stimuli, including pH and glucose. Furthermore, the mechanical properties could be tuned by adjusting the hydrogel composition, thereby facilitating delicate control over mechanotransduction.

Leveraging these properties, we successfully monocultured and differentiated mouse-derived fat (3T3-L1) and muscle (C2C12) cells and bovine-derived primary muscle cells (bMuSC) within mechanically optimized scaffolds. Mature cultures were seamlessly assembled into meat prototypes with customizable marbling patterns and sizes that closely resembled natural red meat without the need for additional treatments or techniques. To the best of our knowledge, this is the first report on the application of self-healing scaffolding technology for the fabrication of marbled cultured meat.

We believe that this technology has the potential to streamline complex production processes, lower high costs associated with cultured meat production, and enhance consumer appeal by improving product quality. Furthermore, implementing self-healing hydrogels as scaffolds can stabilize scaffold connections during bioreactor scale-up and mass production, potentially improving the production efficiency and economic feasibility of cultured meat. These self-healing materials also show promise as superior meat binders to conventional meat adhesives such as transglutaminase, which require extended reaction times and high temperatures but provide insufficient binding strength.[67]

This dynamic system can prime future studies. Investigating cellular movement and signaling dynamics within the system, compared to their irreversibly degradable or physical counterparts can provide valuable insights for optimizing monoculture and scale-up processes.[68] Furthermore, integrating dynamic covalent chemistry into edible scaffolds or combining them with cell-degradable cross-links is a promising approach for the development of novel materials.

4. EXPERIMENTAL SECTION

4.1. Reagents. Information regarding the reagents used in this study is provided in the Supporting Information. All the reagents were stored according to the manufacturer's instructions and used as received. Deionized water was purified using a Milli-Q Integral 3 system (Millipore, USA) to a final resistivity of 18.0 MΩ cm at 25 °C.

4.2. ChsB(OH)$_2$ Synthesis and Characterization. Chitosan (5.0 g, 0.0236 mol anhydroglucosamine) was dissolved in deionized water (500 mL) that was adjusted to pH 4.0−4.5 using 1 M HCl. 3-CPBA (1.958 g, 0.0118 mol) was added to this solution, followed by 1-ethyl-3-(3-(dimethylamino)propyl)carbodiimide hydrochloride (2.262 g, 0.0118 mol) and *N*-hydroxysuccinimide (1.358 g, 0.0118 mol) to initiate conjugation (Scheme S1a). The mixture was stirred for 48 h at room temperature (RT) while maintaining the pH between 4.0 and 4.5. The resulting ChsB(OH)$_2$ was purified using regenerated cellulose dialysis membranes with a 10 kDa molecular weight cutoff (MWCO) (Spectrum Laboratories Spectra/Por 6, Thermo Fisher Scientific, USA) and lyophilized at −50 °C using a freeze-dryer (F8512, ilshinBiobase, S. Korea).

The attenuated total reflectance Fourier-transform infrared (ATR-FTIR) spectrum of ChsB(OH)$_2$ was recorded using an FTIR spectrometer (Nicolet iS50, Thermo Scientific, USA) equipped with a Smart iTR diamond/ZnSe ATR accessory (45° face angle). The spectrum was collected in the 4000−650 cm^{-1} range at a 2 cm^{-1} resolution with 128 scans. The ^{1}H NMR spectrum was acquired using a 600 MHz NMR spectrometer (Avance III HD, Bruker, USA) with 1 wt % DCl in D_2O as the solvent. The UV−visible spectrum of ChsB(OH)$_2$ was recorded using a spectrophotometer (V-770, Jasco, USA). The degree of boronic acid *N*-substitution (*DS*) was calculated using eq 1:

$$DS = \frac{[BA]}{[GlcN]} \times 100\% \tag{1}$$

where $[BA]$ is the boronic acid moiety content (mmol g^{-1}) determined based on absorbance at 285 nm using a calibration curve constructed with 3-CPBA as the standard,[27] and $[GlcN]$ is the anhydroglucosamine content of the starting chitosan with an average deacetylation degree of 80% (4.718 mmol g^{-1}). All UV−visible samples were prepared in 0.1 M HCl.

4.3. ChsB(OH)$_2$/PVA Hydrogel Synthesis. Freeze-dried ChsB-(OH)$_2$ was dissolved in 0.2 M aqueous acetic acid (pH 4.76) at 3 wt % (solution A). PVA was dissolved in deionized water at 10 wt % at 90 °C (solution B). The hydrogels were prepared by mixing solutions A and B in varying volume ratios. The pH of the mixture was adjusted to 7.4 by dropwise addition of 1 M NaOH (10 μL mL^{-1}) to induce cross-linking. The hydrogels were vortexed to remove air bubbles and achieve homogeneity, then stabilized at 4 °C for 24 h to ensure complete cross-linking (**N** series).

To enhance the mechanical properties, the hydrogels underwent a single freeze−thaw cycle, which involved freezing at −20 °C for 6 h followed by thawing at 25 °C for 12 h. This process formed a double network of boronic acid−diol ester and hydrogen bonds within the hydrogel (**F** series).

4.4. Hydrogel Characterization. *4.4.1. Gel Fraction and Equilibrium Swelling Degree.* The lyophilized hydrogels were weighed (W_i), immersed in excess deionized water to rinse the non-cross-linked ChsB(OH)$_2$ and PVA, and then relyophilized until a constant weight (W_e). The gel fraction was calculated using eq 2:[35]

$$\text{Gel fraction (\%)} = \frac{W_e}{W_i} \times 100\% \tag{2}$$

The lyophilized hydrogels were weighed (W_d), immersed in deionized water at RT until equilibrium swelling was reached, blotted dry, and reweighed (W_s). The equilibrium swelling degree (ESD) was calculated using eq 3:[35]

$$\text{ESD (\%)} = \frac{(W_s - W_d)}{W_d} \times 100\% \tag{3}$$

4.4.2. Spectroscopy. The chemical structure of the ChsB(OH)$_2$/PVA hydrogels was analyzed using ATR-FTIR spectroscopy with the same settings as those used for ChsB(OH)$_2$ (Section 4.2).

4.4.3. Scanning Electron Microscopy. The porous structure of the lyophilized hydrogels was examined using field-emission SEM (Sigma 300 VP, Carl Zeiss, Germany). Prior to SEM, the samples were sputter-coated with a platinum (Pt) layer using a turbomolecular pumped coater (Q150 T Plus, Quorum Technologies Ltd., U.K.) operating at 15 mA for 90 s.

4.4.4. Mechanical Testing and Hysteresis. The compressive mechanical properties of the hydrogels were assessed using a universal testing machine (UTM, Instron 5943, U.K.) equipped with a 1 kN load cell at 25 °C. Hydrogel specimens (0.5 cm cubes) were compressed at 5 mm min^{-1}, and the Young's modulus was determined from the slope of the linear region (<10% strain) in the stress−strain curve.

The hysteresis of the hydrogel was examined via cyclic compression testing using the same UTM. Specimens (0.5 cm cubes) were compressed and unloaded at 50 mm min^{-1} to 50% strain for 100 cycles, with a 10 s relaxation between cycles. The hysteresis energy was calculated by subtracting the unloading energy density (integrated area under the unloading curve) from the loading energy density (integrated area under the loading curve). The percentage of energy dissipated was calculated as the ratio of the hysteresis energy to the loading energy density.

4.4.5. Self-Healing, Responsiveness, and Rheological Properties. The self-healing ability of the hydrogels was observed under a light

https://doi.org/10.1021/acsami.5c03479
ACS Appl. Mater. Interfaces 2025, 17, 31881−31897

microscope (AxioCam MRc 5, Zeiss, Germany). pH responsiveness was assessed by exposing stabilized hydrogels to acidic pH (1 M HCl) or neutral/basic pH (1 M NaOH) to disrupt and reform the boronic acid−diol ester linkages, respectively. The responsiveness to DMEM containing 0.45 wt % glucose and 5 wt % glucose solution was evaluated to assess their suitability as scaffolds for cell culture.

The rheological properties were measured using a modular compact rotating rheometer (MCR 302, Anton Paar, Austria) equipped with 25 mm stainless-steel parallel plates. Specimens (~1 mm high × 25 mm wide) were subjected to a 0.1−10 Hz frequency sweep at 10% strain. The storage (G') and loss (G'') moduli were recorded at pH 4.5, 6.5, and 7.5. Furthermore, the G′ of 24 h-cured hydrogels exposed to 0.45 and 5 wt % glucose solutions were measured at pH 7.5. All tests were conducted at 25 °C.

4.5. Quantification of the Boronic Acid−Diol Interaction Energy at the Molecular Level. Atomically smooth mica surfaces were exfoliated from ruby muscovite (grade 1, S&J Trading Inc., USA) in a dust-free laminar-flow hood. Each 1 cm × 1 cm mica piece was then coated with a silver layer (~5 nm thick) using an E-beam evaporator (KVE-C300160, Korea Vacuum Tech). The coated mica sheets were glued (silver-coated side facing downward) onto cylindrical silica disks (radius of curvature, R = 2 cm) using epoxy resin glue (EPON 1004F, Exxon Chemicals, USA), which was cured under UV at RT for 30 min. The disks were then mounted in the SFA according to the configuration shown in Figure S13.

Separate solutions of chitosan and $ChsB(OH)_2$ were prepared at 50 $\mu g\ mL^{-1}$ in sodium acetate buffer (10 mM, pH 4). Each solution was filtered through a 0.45 μm poly(vinylidene fluoride) (PVDF) syringe filter (Millipore, USA). A 40 μL aliquot of the filtered solution was applied dropwise onto the mica surface and left undisturbed for 30 min at RT. The unbound molecules were thoroughly rinsed with sodium acetate buffer.

The intermolecular force−distance functions, $F(D)$, between the two surfaces, $ChsB(OH)_2$ vs mica, and chitosan vs mica, were determined using an SFA 2000 (Surforce LLC, USA). Measurements were conducted at pH 4 (0.1 M acetate buffer) and pH 7 (0.1 M Dulbecco's phosphate-buffered saline, DPBS). The surface-separation distance was monitored using multiple-beam interferometry, which generated fringes of equal chromatic order from a back-silvered mirror layer. The mica−mica contact distance in air was used as the reference distance (D = 0). The coated mica surface was brought into molecular contact with the uncoated surface at the steric wall distance, D_{SW}. After 30 s of equilibrium, the surfaces were progressively separated until they abruptly detached. The separation distance at this point was used to calculate the adhesion force (F_{ad}) using Hooke's law. The Derjaguin approximation was applied to relate the force (F) between two spheres of equal radius (R), normalized by the radius (F/R), to energy per unit area (W) of two flat surfaces at the same D. The Johnson−Kendall−Roberts theory was used to calculate the adhesion energy per unit area ($W_{ad} = F_{ad}/1.5\pi R$) for soft and elastic surfaces.[45] Force−distance profiles were obtained at four positions.

4.6. Cell Handling. 3T3-L1 and C2C12 cells were obtained from the American Type Culture Collection (ATCC, https://www.atcc.org/) and handled according to the manufacturer' protocols. Primary muscle cells from Hanwoo cattle (bMuSC) were purchased from Seawith (S. Korea). The growth media for 3T3-L1, C2C12, and bMuSC consisted of DMEM supplemented with antibiotics (100 units mL^{-1} penicillin and 100 $\mu g\ mL^{-1}$ streptomycin), and serum [10 v% bovine calf serum for 3T3-L1, and 10 v% fetal bovine serum (FBS) for C2C12 and bMuSC]. Cell cultures were maintained in a 5 v% CO_2 incubator at 37 °C and subcultured before reaching 80% confluence. The cell passage number was kept below ten to preserve regular morphology and differentiation potential.

4.7. Cell Experiments. Because of the slower growth compared to the two immortalized cells, bMuSC cells were seeded at twice the density of C2C12 and 3T3-L1 cells, unless otherwise specified. The cell densities provided below apply to C2C12 and 3T3-L1 cells.

4.7.1. Hydrogel Biocompatibility (Cytotoxicity). 4.7.1.1. WST-8 (CCK-8) Assay. The cytotoxicity of the hydrogel components [$ChsB(OH)_2$ and PVA] was evaluated according to ISO-10993-5 and ISO-10993-5-12 standards using CCK-8 (Dojindo Laboratories, Japan). Freeze-dried test materials were extracted in cell culture media (0.2 g mL^{-1}) at 37 °C for 24 h with agitation (100 rpm), and the extracts were applied on the target cells. Growth media, low-density polyethylene strip extract (0.2 g mL^{-1}) and zinc diethyldithiocarbamate (500 μM) served as blank, negative and positive controls, respectively.

Cells (10 μL, 10^5 cells mL^{-1}) were seeded in a 96-well plate (SPL Life Science, S. Korea) and allowed to proliferate in growth media (90 μL) for 24 h. The media were then replaced with the test extracts (100 μL) and incubated for another 24 h. After rinsing three times with DPBS, the cells were incubated in DMEM containing 10 v% CCK-8 reagent without phenol red at 37 °C for 1 h. Viable cells reduced the WST-8 salt to orange formazan, which was quantified by measuring absorbance at 450 nm (optical density OD 450) using a microplate reader (Hidex Sense, Finland).[48] Cell viability relative to the blank was calculated using eq 4:

$$\text{Viability}\ (\%) = \frac{OD_s}{OD_b} \times 100\% \tag{4}$$

where OD_s and OD_b are the measured (OD 450−OD 650) values of the test sample extract and blank, respectively. The 650 nm reference wavelength was subtracted to correct for interference from precipitated proteins and cellular debris.

4.7.1.2. Cell Proliferation. Cell proliferation in hydrogels over 1 week was monitored using the CCK-8 assay. The hydrogels were purified by dialysis against DPBS using 10 kDa MWCO regenerated cellulose membranes. Cells (500 μL, 10^6 cells mL^{-1}) were seeded on top of hydrogel scaffolds (~0.3−0.5 cm thick) that were pre-equilibrated with growth media in a 24-well plate. Growth media (500 μL) was added and refreshed daily. To minimize hydrogel interference, the reacted CCK-8 solution was transferred to a new 96-well plate before OD 450 measurement, eliminating the need for 650 nm subtraction. Fresh growth media were replenished for further experimentation.

4.7.1.3. Fluorescence Imaging and Quantification. Cell viability was visually assessed using a LIVE/DEAD viability/cytotoxicity kit for mammalian cells. Cells (500 μL, 10^6 cells mL^{-1}) were seeded on hydrogel scaffolds (<0.3 cm thick) in a 24-well plate, topped with growth media (500 μL), and cultured for 3 days. After rinsing three times with DPBS, the cells were stained with calcein acetoxymethyl ester (2 μM in DPBS) for viable cells and ethidium homodimer-1 (EthD-1, 4 μM in DPBS) for dead cells at 37 °C for 30 min in the dark. Nuclei were stained with Hoechst 33342 (5 $\mu g\ mL^{-1}$ in DPBS) at 37 °C for 5 min in the dark, followed by a single DPBS rinse (500 μL per well). After staining, the hydrogels were sectioned and transferred to a confocal dish (SPL Life Science, S. Korea) for imaging using a laser confocal microscope (LSM 780, Carl Zeiss AG, Germany) with the following parameters: calcein (laser power 0.1−2%, excitation 495 nm, emission 530 nm, green), EthD-1 (laser power 0.1−5%, excitation 528 nm, emission 645 nm, red), and Hoechst 33342 (laser power 1−5%, excitation 350 nm, emission 461 nm, blue).

The fluorescence intensity of calcein (proportional to the viable cell numbers) was measured using the Sense microplate reader, and cell viability was calculated using eq 5:

$$\text{Viability}\ \% = \frac{F_{530sam} - F_{530min}}{F_{530max} - F_{530min}} \times 100\% \tag{5}$$

where $F_{530\ sam}$ is the 530 nm fluorescence intensity of the sample labeled with both dyes, and $F_{530\ max}$ and $F_{530\ min}$ are the 530 nm fluorescence intensities of the samples assumed to contain all viable or dead cells, labeled with calcein or EthD-1, respectively. Single-labeled samples were prepared by culturing cells on polystyrene well plates. Cell viability and proliferation in the hydrogel scaffolds were compared to those in Matrigel (5 mg mL^{-1}, 354230, Corning, USA).[49]

4.7.2. Cell Differentiation. Cells (1 mL, 10^6 cells mL^{-1} suspension) were seeded on the hydrogel scaffold that supported the highest

https://doi.org/10.1021/acsami.5c03479
ACS Appl. Mater. Interfaces 2025, 17, 31881−31897

proliferation rate for each cell type (**N1** for C2C12 and bMuSC, and **F0.5** for 3T3-L1) in a six-well plate. The cells were cultured until they reached confluence to ensure sufficient intercellular signaling for differentiation.

Confluent 3T3-L1 cells were driven toward adipogenic differentiation using an adipogenic differentiation medium for 3 days, followed by maintenance in an adipocyte maintenance medium, which was refreshed daily. The adipogenic differentiation medium contained DMEM supplemented with FBS (10 v%), dexamethasone (1.0 μM), 3-isobutyl-1-methylxanthine (0.5 mM), and insulin (1 μg mL^{-1}). The adipocyte maintenance medium contained DMEM supplemented with FBS (10 v%) and insulin (1 μg mL^{-1}). Confluent C2C12 cells were driven toward myogenic differentiation and maintained in DMEM containing donor equine serum (2 v%) and insulin (1 μg mL^{-1}) with daily refreshment. Confluent bMuSC cells were driven toward myogenic differentiation and maintained in DMEM containing insulin (1 μg mL^{-1}) with daily refreshment. All media contained penicillin (100 units mL^{-1}) and streptomycin (100 μg mL^{-1}).

4.7.3. Fluorescence Microscopy of Differentiated Cells. 4.7.3.1. Adipogenic Differentiation. Nile Red staining was performed to visualize intracellular lipid (triglyceride) droplets in differentiated 3T3-L1 adipocytes. The cells were fixed with paraformaldehyde (4 w % in DPBS, RT, 20 min), incubated with Nile Red (0.5 μg mL^{-1} in DPBS, 37 °C, 30 min), and counterstained with Hoechst 33342 (5 μg mL^{-1} in DPBS, 37 °C, 5 min). Due to its poor water solubility, a Nile Red stock solution (500 μg mL^{-1}) was prepared in dimethyl sulfoxide (DMSO) and diluted in DPBS for staining. Stained cells were rinsed three times with DPBS and observed using the LSM 780 microscope with the following settings: Nile Red (laser power 1−5%, excitation 559 nm, emission 635 nm, red) and Hoechst 33342 (laser power 1−5%, excitation 350 nm, emission 461 nm, blue). The Nile Red fluorescence intensity at 635 nm was quantified using the Sense microplate reader to assess lipid production. In this experiment, cells (500 μL, 10^6 cells mL^{-1}) were seeded on hydrogels in a 24-well plate and topped with media (500 μL). Nile Red (0.5 μg mL^{-1}) was dissolved in DMSO as a dye carrier to enhance fluorescence intensity measurements.

4.7.3.2. Myogenic Differentiation. MHC staining was performed to observe the C2C12 and bMuSC myotubes. Cells were fixed with formaldehyde (8 w% in DPBS, RT, 20 min), permeabilized with Triton X-100 (0.1 v% in DPBS, RT, 20 min), and blocked with bovine serum albumin (BSA, 1 w% in DPBS, RT, 1 h). They were incubated in DPBS containing myosin 4 antibody MF20 (0.625 μg mL^{-1}) and BSA (1 wt %) at 4 °C overnight, rinsed with DPBS, and incubated in DPBS containing goat antimouse IgG, IgM (H+L) secondary antibody conjugated to Alexa Fluor 488 (0.2 μg mL^{-1}) and BSA (1 wt %) at RT for 1 h. Nuclei were counterstained with Hoechst 33342 (5 μg mL^{-1} in DPBS, 37 °C, 5 min). After rinsing three times with DPBS, the stained cells were observed using the LMS 780 microscope with the following settings: Alexa Fluor 488 (laser power 0.1−6%, excitation 488 nm, emission 525 nm, green) and Hoechst 33342 (laser power 1−5%, excitation 350 nm, emission 461 nm, blue).

All cultures were imaged at the hydrogel cross sections to assess cell migration from the surface to the interior, as well as cell growth and differentiation within the hydrogel.

4.7.4. Image Analysis. Confocal images were analyzed using ImageJ (National Institute of Health, https://imagej.net/). To measure C2C12 myotube dimensions and 3T3-L1 lipid droplet sizes, a scale bar of known length was used for pixel-to-distance calibration. The software converted 100 pixel-counts into myotube lengths and widths and lipid droplet maximum diameters.

For myotube fusion analysis, nuclei were considered part of a fused myotube if their nearest neighbor distance was less than 3 μm border-to-border. The fusion index was calculated as the ratio of nuclei within the MHC-stained myotubes to the total number of nuclei in the field. Myotube alignment was assessed by measuring the relative angle shift between the lengths of the surrounding and central myotubes in the field (100 measurements). The myotubes used in the analysis contained at least two nuclei.[69]

The relative lipid synthesis per cell was determined by normalizing the total pixel area of the lipid signal (red) to that of the nucleus signal (blue). Only pixels with a signal intensity above 15,000 were considered.

4.7.5. Gel Electrophoresis and Western Blot. C2C12 and 3T3-L1 cells were monocultured on the hydrogels in a six-well plate (10^6 cells per well) and allowed to differentiate. After medium aspiration, the cells were rinsed three times with ice-cold DPBS and lysed using a radioimmunoprecipitation assay buffer (200 μL per well) at 4 °C for 30 min. The lysates were centrifuged at 15,000 rpm for 15 min at 4 °C using a benchtop centrifuge (Allegra 64R, Beckman Coulter, USA) to collect protein lysate supernatants. Total protein concentrations were quantified using the Pierce Bradford Plus protein assay kit with a BSA standard curve (125−1500 μg mL^{-1}).

Proteins were denatured in Laemmli buffer at 95 °C for 5 min. The 2X buffer (10 mL) contained 0.5 M Tris−HCl (pH 6.8, 2.5 mL), glycerol (2 mL), 10 w/v% sodium dodecyl sulfate (SDS) aqueous solution (4 mL), 0.1 w/v% bromophenol blue solution (0.5 mL), and β-mercaptoethanol (1 mL). Denatured proteins were separated via SDS−polyacrylamide gel electrophoresis at 120 V for 2.5 h following an initial run at 60 V for 15 min, using a Mini-PROTEAN Tetra Vertical Cell (Bio-Rad Laboratories, USA). The electrophoresis buffer was maintained at a 15−20 °C. C2C12 and 3T3-L1 proteins were resolved using 8 and 12 wt % gels, respectively. The gel compositions are listed in Table S6.

The separated proteins were transferred to a methanol-activated PVDF membrane (LC2002, Thermo Fisher Scientific, USA) using a Mini Trans-Blot Cell (Bio-Rad Laboratories, USA) at 100 V for 1 h in an ice/water cooling bath. The 1X transfer buffer consisted of Tris base (0.48 mM), glycine (3.84 mM) and methanol (20 v%).

After transfer, the membrane was blocked with 3 wt % BSA in Tris-buffered saline (pH 7.6) containing Tween 20 (TBST). The 1X TBST (1 L) contained Tris base (2.4 g), sodium chloride (8.8 g), and Tween 20 (0.1 v%). The membrane was immunoblotted with a primary antibody at 4 °C for 12 h, rinsed three times (10 min each) with TBST, followed by incubation with horseradish peroxidase (HRP)-conjugated secondary antibodies, and rinsed six more times (10 min each) with TBST. Antibodies were diluted in TBST containing 3 wt % BSA to the following final concentrations: β-actin (0.5 μg mL^{-1}), MF20 (1 μg mL^{-1}), PPARγ (0.2 μg mL^{-1}), FABP4 (0.5 μg mL^{-1}), and secondary antibodies (β-actin: 0.02 μg mL^{-1}, others: 0.05 μg mL^{-1}).

Immunoreactive blots were visualized by incubating the membrane in a SuperSignal West Pico PLUS HPR chemiluminescent substrate containing an enhancer for 5 min. Images were captured using a Gel Doc XR System (Bio-Rad Laboratories, USA). Protein expression was quantified by measuring the blot intensity using Image Lab (Bio-Rad Laboratories, USA).

4.7.6. Meat Prototype Construction and Tissue Culture Characterization. After 28 d of differentiation, adipose- and muscle-like tissues were assembled into cultured meat constructs via hydrogel self-healing. Muscle-like tissue was distinguished from adipose-like tissue by carmine staining, which imparted a reddish color to the muscle. The muscle/fat assembly was wetted with DMEM and stabilized at RT for 1 h to ensure complete interfacial adhesion.

For composition analysis, fully swollen **N1** and **F0.5** hydrogels were weighed before cell seeding. After differentiation for 28 d, the cultures (**N1** + C2C12 cells and **F0.5** + 3T3-L1 cells) were weighed after removing culture media, rinsing with deionized water and blotting dry. The cultures were then lyophilized to a constant weight to determine water and dry matter contents. As the dried hydrogel content could be calculated from the ESD data, the tissue dry weight was obtained by subtracting the dried hydrogel and water weights from the total weight, assuming no hydrogel degradation during the culture period. The dry hydrogel contents were <5 and <10 wt % for the C2C12/**N1** and 3T3-L1/**F0.5** cultures, respectively.

https://doi.org/10.1021/acsami.5c03479
ACS Appl. Mater. Interfaces 2025, 17, 31881−31897

Nutritional analysis of the wet cultures was conducted by CHEILLAB (S. Korea), an institution certified for testing food and livestock products. Total protein was measured by digesting the samples in sulfuric acid (H_2SO_4), distilling with NaOH, and titrating using HCl. The fatty acid composition was determined using gas chromatography with flame ionization detection.

Elemental analysis of the dried samples was conducted using a Unicube elemental analyzer (Elementar, Germany) for hydrogen (H), carbon (C), nitrogen (N), and sulfur (S), and a Flash 2000 elemental analyzer (Thermo Scientific, USA) for oxygen (O). Samples for boron (B) content analysis (0.1 g) were pulverized in liquid nitrogen, suspended in deionized water (100 mL) using tip sonication (40% amplitude, 5 s on/2 s off, RT, 3 min), and filtered through fritted glass (porosity 4) under reduced pressure to remove the metallic clusters released from the sonication probe. The suspension was analyzed using inductively coupled plasma-atomic emission spectrometry (iCAP 6500 Duo, Thermo Fisher Scientific, USA).

■ ASSOCIATED CONTENT

Supporting Information

The Supporting Information is available free of charge at https://pubs.acs.org/doi/10.1021/acsami.5c03479.

Reagent information; reaction scheme for conjugating 3-CPBA to chitosan; characterization data of $ChsB(OH)_2$: FTIR, ^1H NMR and UV−visible spectra, and compressive mechanical properties; synthesis and characterization data of $ChsB(OH)_2$/PVA hydrogels: gel fraction, IR spectra, porous structure, equilibrium swelling degree, compressive mechanical properties and hysteresis, and rheological behavior in response to pH change and glucose; SFA experimental set up; cellular experiment data: growth of 3T3-L1 and C2C12 in $ChsB(OH)_2$/PVA hydrogels, western blot images, and postdifferentiation fatty acid content and elemental composition analyses; and electrophoresis gel composition (PDF)

Light microscopy showing the self-healing progress of microcracks in the **N1** hydrogel during the first and fifth healing cycles (MP4)

Response of the **N1** hydrogel to DMEM and the 5.0 wt % glucose solution (MP4)

Stretching of an edge-to-edge-fused meat prototype before and after frying (MP4)

■ AUTHOR INFORMATION

Corresponding Authors

Jeyoung Park − *Department of Chemical and Biomolecular Engineering, Sogang University, Seoul 04107, Republic of Korea;* orcid.org/0000-0002-9369-1597; Email: jeypark@sogang.ac.kr

Hyo Jeong Kim − *Research Center for Bio-based Chemistry, Korea Research Institute of Chemical Technology (KRICT), Ulsan 44429, Republic of Korea; Advanced Materials and Chemical Engineering, Korea National University of Science and Technology (UST), Daejeon 34113, Republic of Korea;* orcid.org/0000-0002-5331-5407; Email: khjkye@krict.re.kr

Dongyeop X. Oh − *Department of Polymer Science and Engineering and Program in Environmental and Polymer Engineering, Inha University, Incheon 22212, Republic of Korea;* orcid.org/0000-0003-3665-405X; Email: d.oh@inha.ac.kr

Authors

Lam Tan Hao − *Research Center for Bio-based Chemistry, Korea Research Institute of Chemical Technology (KRICT), Ulsan 44429, Republic of Korea;* orcid.org/0000-0001-9791-6071

Seunghyeon Lee − *Division of Environmental Science and Engineering, Pohang University of Science and Technology (POSTECH), Pohang 37673, Republic of Korea*

Dong Soo Hwang − *Division of Environmental Science and Engineering, Pohang University of Science and Technology (POSTECH), Pohang 37673, Republic of Korea;* orcid.org/0000-0002-2487-2255

Hyeonyeol Jeon − *Research Center for Bio-based Chemistry, Korea Research Institute of Chemical Technology (KRICT), Ulsan 44429, Republic of Korea; Advanced Materials and Chemical Engineering, Korea National University of Science and Technology (UST), Daejeon 34113, Republic of Korea;* orcid.org/0000-0001-9176-2913

Complete contact information is available at: https://pubs.acs.org/10.1021/acsami.5c03479

Author Contributions

L.T.H.: Conceptualization, Data curation, Formal analysis, Methodology, Visualization, Writing—original draft, Writing—review and editing. S.L.: Data curation, Formal analysis, Investigation, Methodology, Resources, Validation, Visualization, Writing—original draft. D.S.H.: Formal analysis, Methodology, Resources, Validation, Writing—review and editing. H.J.: Funding acquisition, Resources, Writing—review and editing. J.P.: Funding acquisition, Project administration, Supervision, Validation, Writing—original draft, Writing—review and editing. H.J.K.: Conceptualization, Formal analysis, Funding acquisition, Methodology, Project administration, Resources, Supervision, Validation, Writing—original draft, Writing—review and editing. D.X.O.: Conceptualization, Funding acquisition, Investigation, Methodology, Project administration, Resources, Supervision, Validation, Visualization, Writing—original draft, Writing—review and editing. All authors have given approval to the final version of the manuscript.

Notes

The authors declare no competing financial interest.

■ ACKNOWLEDGMENTS

This research was supported by the National Research Foundation (NRF), funded by the Ministry of Science and ICT of South Korea (grant 2022M3H4A1A03076577), and the Nano & Material Technology Development Program through the NRF, funded by the Ministry of Science and ICT (grant RS-2024-00408795). H.J.K. gratefully acknowledges the support from the Korea Research Institute of Chemical Technology (KRICT) core project (grant KS2542-10), and the High Value-added Food Technology Development Program, funded by the Korea Institute of Planning and Evaluation for Technology in Food, Agriculture, and Forestry under the Ministry of Agriculture, Food and Rural Affairs (MAFRA) of South Korea (grant RS-2024-00509809). L.T.H. thanks Jinhoe Hur (Ulsan National Institute of Science and Technology, UNIST) for technical confocal microscopy guidance, and Ju Young Lee and So Hee Son (KRICT) for providing the experimental equipment used for the western blot analyses.

ABBREVIATIONS

3D, three-dimension(al); 3-CPBA, 3-carboxyphenylboronic acid; ATR-FTIR, attenuated total reflectance Fourier-transform infrared; BSA, bovine serum albumin; CCK-8, Cell Counting Kit-8; DMEM, Dulbecco's modified Eagle's medium; DMSO, dimethyl sulfoxide; DPBS, Dulbecco's phosphate-buffered saline; ECM, extracellular matrix; ESD, equilibrium swelling degree; EthD-1, ethidium homodimer-1; FABP-4, fatty acid-binding protein 4; FBS, fetal bovine serum; HRP, horseradish peroxidase; IPN, interpenetrating network; MHC, myosin heavy chain; MWCO, molecular weight cutoff; ND, not detected; NMR, nuclear magnetic resonance; PPAR-γ, peroxisome proliferator-activated receptor gamma; PVA, poly(vinyl alcohol); PVDF, poly(vinylidene fluoride); RT, room temperature; SDS, sodium dodecyl sulfate; SEM, scanning electron microscopy; SFA, surface forces apparatus; TBST, Tris-buffered saline containing Tween 20; UTM, universal testing machine; UV, ultraviolet; WST-8, water-soluble tetrazolium

REFERENCES

(1) Leroy, F.; Smith, N. W.; Adesogan, A. T.; Beal, T.; Iannotti, L.; Moughan, P. J.; Mann, N. The Role of Meat in the Human Diet: Evolutionary Aspects and Nutritional Value. *Anim. Front.* **2023**, *13* (2), 11−18.

(2) Santos, D.; Monteiro, M. J.; Voss, H.-P.; Komora, N.; Teixeira, P.; Pintado, M. The Most Important Attributes of Beef Sensory Quality and Production Variables That Can Affect It: a Review. *Livest. Sci.* **2021**, *250*, No. 104573.

(3) Polkinghorne, R. J.; Thompson, J. M. Meat Standards and Grading. *Meat Sci.* **2010**, *86* (1), 227−235.

(4) Godfray, H. C. J.; Aveyard, P.; Garnett, T.; Hall, J. W.; Key, T. J.; Lorimer, J.; Pierrehumbert, R. T.; Scarborough, P.; Springmann, M.; Jebb, S. A. Meat Consumption, Health, and the Environment. *Science* **2018**, *361* (6399), No. eaam5324.

(5) Tuomisto, H. L.; Teixeira de Mattos, M. J. Environmental Impacts of Cultured Meat Production. *Environ. Sci. Technol.* **2011**, *45* (14), 6117−6123.

(6) Bryant, C. J. Culture, Meat, and Cultured Meat. *J. Anim. Sci.* **2020**, *98* (8), No. skaa172.

(7) Post, M. J.; Levenberg, S.; Kaplan, D. L.; Genovese, N.; Fu, J.; Bryant, C. J.; Negowetti, N.; Verzijden, K.; Moutsatsou, P. Scientific, Sustainability and Regulatory Challenges of Cultured Meat. *Nat. Food* **2020**, *1* (7), 403−415.

(8) Zagury, Y.; Ianovici, I.; Landau, S.; Lavon, N.; Levenberg, S. Engineered Marble-Like Bovine Fat Tissue for Cultured Meat. *Commun. Biol.* **2022**, *5* (1), 927.

(9) Ye, Y.; Zhou, J.; Guan, X.; Sun, X. Commercialization of Cultured Meat Products: Current Status, Challenges, and Strategic Prospects. *Future Foods* **2022**, *6*, No. 100177.

(10) Lee, M.; Park, S.; Choi, B.; Choi, W.; Lee, H.; Lee, J. M.; Lee, S. T.; Yoo, K. H.; Han, D.; Bang, G.; Hwang, H.; Koh, W.-G.; Lee, S.; Hong, J. Cultured Meat with Enriched Organoleptic Properties by Regulating Cell Differentiation. *Nat. Commun.* **2024**, *15* (1), 77.

(11) David, S.; Tsukerman, A.; Safina, D.; Maor-Shoshani, A.; Lavon, N.; Levenberg, S. Co-Culture Approaches for Cultivated Meat Production. *Nat. Rev. Bioeng.* **2023**, *1* (11), 817−831.

(12) Goers, L.; Freemont, P.; Polizzi, K. M. Co-Culture Systems and Technologies: Taking Synthetic Biology to the Next Level. *J. R. Soc. Interface* **2014**, *11* (96), 20140065.

(13) Onoe, H.; Okitsu, T.; Itou, A.; Kato-Negishi, M.; Gojo, R.; Kiriya, D.; Sato, K.; Miura, S.; Iwanaga, S.; Kuribayashi-Shigetomi, K.; Matsunaga, Y. T.; Shimoyama, Y.; Takeuchi, S. Metre-Long Cell-Laden Microfibres Exhibit Tissue Morphologies and Functions. *Nat. Mater.* **2013**, *12* (6), 584−590.

(14) Kang, D.-H.; Louis, F.; Liu, H.; Shimoda, H.; Nishiyama, Y.; Nozawa, H.; Kakitani, M.; Takagi, D.; Kasa, D.; Nagamori, E.; Irie, S.; Kitano, S.; Matsusaki, M. Engineered Whole Cut Meat-Like Tissue by the Assembly of Cell Fibers Using Tendon-Gel Integrated Bioprinting. *Nat. Commun.* **2021**, *12* (1), 5059.

(15) Caliari, S. R.; Burdick, J. A. A Practical Guide to Hydrogels for Cell Culture. *Nat. Methods* **2016**, *13* (5), 405−414.

(16) Bomkamp, C.; Skaalure, S. C.; Fernando, G. F.; Ben-Arye, T.; Swartz, E. W.; Specht, E. A. Scaffolding Biomaterials for 3D Cultivated Meat: Prospects and Challenges. *Adv. Sci.* **2022**, *9* (3), No. 2102908.

(17) Bertsch, P.; Diba, M.; Mooney, D. J.; Leeuwenburgh, S. C. G. Self-Healing Injectable Hydrogels for Tissue Regeneration. *Chem. Rev.* **2023**, *123* (2), 834−873.

(18) Diesendruck, C. E.; Sottos, N. R.; Moore, J. S.; White, S. R. Biomimetic Self-Healing. *Angew. Chem., Int. Ed.* **2015**, *54* (36), 10428−10447.

(19) Niu, W.; Zhu, Y.; Wang, R.; Lu, Z.; Liu, X.; Sun, J. Remalleable, Healable, and Highly Sustainable Supramolecular Polymeric Materials Combining Superhigh Strength and Ultrahigh Toughness. *ACS Appl. Mater. Interfaces* **2020**, *12* (27), 30805−30814.

(20) Wang, S.; Urban, M. W. Self-Healing Polymers. *Nat. Rev. Mater.* **2020**, *5* (8), 562−583.

(21) Holten-Andersen, N.; Harrington, M. J.; Birkedal, H.; Lee, B. P.; Messersmith, P. B.; Lee, K. Y. C.; Waite, J. H. pH-Induced Metal-Ligand Cross-Links Inspired by Mussel Yield Self-Healing Polymer Networks with near-Covalent Elastic Moduli. *Proc. Nat. Acad. Sci.* **2011**, *108* (7), 2651−2655.

(22) Cho, S.; Hwang, S. Y.; Oh, D. X.; Park, J. Recent Progress in Self-Healing Polymers and Hydrogels Based on Reversible Dynamic B−O Bonds: Boronic/Boronate Esters, Borax, and Benzoxaborole. *J. Mater. Chem. A* **2021**, *9* (26), 14630−14655.

(23) Yang, H.-S.; Cho, S.; Eom, Y.; Park, S.-A.; Hwang, S. Y.; Jeon, H.; Oh, D. X.; Park, J. Preparation of Self-Healable and Spinnable Hydrogel by Dynamic Boronate Ester Bond from Hyperbranched Polyglycerol and Boronic Acid-Containing Polymer. *Macromol. Res.* **2021**, *29* (2), 140−148.

(24) Deng, C. C.; Brooks, W. L. A.; Abboud, K. A.; Sumerlin, B. S. Boronic Acid-Based Hydrogels Undergo Self-Healing at Neutral and Acidic pH. *ACS Macro Lett.* **2015**, *4* (2), 220−224.

(25) Chen, Y.; Diaz-Dussan, D.; Wu, D.; Wang, W.; Peng, Y.-Y.; Asha, A. B.; Hall, D. G.; Ishihara, K.; Narain, R. Bioinspired Self-Healing Hydrogel Based on Benzoxaborole-Catechol Dynamic Covalent Chemistry for 3D Cell Encapsulation. *ACS Macro Lett.* **2018**, *7* (8), 904−908.

(26) Pettignano, A.; Grijalvo, S.; Häring, M.; Eritja, R.; Tanchoux, N.; Quignard, F.; Díaz Díaz, D. Boronic Acid-Modified Alginate Enables Direct Formation of Injectable, Self-Healing and Multi-stimuli-Responsive Hydrogels. *Chem. Commun.* **2017**, *53* (23), 3350−3353.

(27) Hong, S. H.; Kim, S.; Park, J. P.; Shin, M.; Kim, K.; Ryu, J. H.; Lee, H. Dynamic Bonds between Boronic Acid and Alginate: Hydrogels with Stretchable, Self-Healing, Stimuli-Responsive, Remoldable, and Adhesive Properties. *Biomacromolecules* **2018**, *19* (6), 2053−2061.

(28) He, C.; Dong, J.; Xu, C.; Pan, X. N-Coordinated Organoboron in Polymer Synthesis and Material Science. *ACS Polym. Au* **2023**, *3* (1), 5−27.

(29) Lee, S.; Hao, L. T.; Park, J.; Oh, D. X.; Hwang, D. S. Nanochitin and Nanochitosan: Chitin Nanostructure Engineering with Multiscale Properties for Biomedical and Environmental Applications. *Adv. Mater.* **2023**, *35* (4), No. 2203325.

(30) Musah, S.; Morin, S. A.; Wrighton, P. J.; Zwick, D. B.; Jin, S.; Kiessling, L. L. Glycosaminoglycan-Binding Hydrogels Enable Mechanical Control of Human Pluripotent Stem Cell Self-Renewal. *ACS Nano* **2012**, *6* (11), 10168−10177.

(31) Thiele, J.; Ma, Y.; Bruekers, S. M. C.; Ma, S.; Huck, W. T. S. 25th Anniversary Article: Designer Hydrogels for Cell Cultures: a Materials Selection Guide. *Adv. Mater.* **2014**, *26* (1), 125−148.

https://doi.org/10.1021/acsami.5c03479
ACS Appl. Mater. Interfaces 2025, 17, 31881−31897

(32) Stauffer, S. R.; Peppast, N. A. Poly(Vinyl Alcohol) Hydrogels Prepared by Freezing-Thawing Cyclic Processing. *Polymer* **1992**, *33* (18), 3932−3936.
(33) Duval, K.; Grover, H.; Han, L.-H.; Mou, Y.; Pegoraro, A. F.; Fredberg, J.; Chen, Z. Modeling Physiological Events in 2D vs. 3D Cell Culture. *Physiology* **2017**, *32* (4), 266−277.
(34) Wang, L.; Wang, X.; Feng, S.; Li, L. Dynamic Boronic Ester Cross-Linked Polymers with Tunable Properties via Side-Group Engineering. *Polymers* **2024**, *16* (24), 3567.
(35) Ghobril, C.; Grinstaff, M. W. The Chemistry and Engineering of Polymeric Hydrogel Adhesives for Wound Closure: a Tutorial. *Chem. Soc. Rev.* **2015**, *44* (7), 1820−1835.
(36) Gupta, S.; Goswami, S.; Sinha, A. A Combined Effect of Freeze−Thaw Cycles and Polymer Concentration on the Structure and Mechanical Properties of Transparent PVA Gels. *Biomed. Mater.* **2012**, *7* (1), No. 15006.
(37) Levental, I.; Georges, P. C.; Janmey, P. A. Soft Biological Materials and Their Impact on Cell Function. *Soft Matter* **2007**, *3* (3), 299−306.
(38) Guimarães, C. F.; Gasperini, L.; Marques, A. P.; Reis, R. L. The Stiffness of Living Tissues and Its Implications for Tissue Engineering. *Nat. Rev. Mater.* **2020**, *5* (5), 351−370.
(39) Fuchs, S.; Shariati, K.; Ma, M. Specialty Tough Hydrogels and Their Biomedical Applications. *Adv. Healthcare Mater.* **2020**, *9* (2), No. 1901396.
(40) Zhou, X.; Guo, B.; Zhang, L.; Hu, G.-H. Progress in Bio-Inspired Sacrificial Bonds in Artificial Polymeric Materials. *Chem. Soc. Rev.* **2017**, *46* (20), 6301−6329.
(41) Eom, Y.; Kim, S.-M.; Lee, M.; Jeon, H.; Park, J.; Lee, E. S.; Hwang, S. Y.; Park, J.; Oh, D. X. Mechano-Responsive Hydrogen-Bonding Array of Thermoplastic Polyurethane Elastomer Captures Both Strength and Self-Healing. *Nat. Commun.* **2021**, *12* (1), 621.
(42) Tuladhar, A.; Chase, Z. A.; Baer, M. D.; Legg, B. A.; Tao, J.; Zhang, S.; Winkelman, A. D.; Wang, Z.; Mundy, C. J.; De Yoreo, J. J.; Wang, H. Direct Observation of the Orientational Anisotropy of Buried Hydroxyl Groups inside Muscovite Mica. *J. Am. Chem. Soc.* **2019**, *141* (5), 2135−2142.
(43) Lee, D. W.; Lim, C.; Israelachvili, J. N.; Hwang, D. S. Strong Adhesion and Cohesion of Chitosan in Aqueous Solutions. *Langmuir* **2013**, *29* (46), 14222−14229.
(44) Lim, C.; Lee, D. W.; Israelachvili, J. N.; Jho, Y.; Hwang, D. S. Contact Time- and pH-Dependent Adhesion and Cohesion of Low Molecular Weight Chitosan Coated Surfaces. *Carbohydr. Polym.* **2015**, *117*, 887−894.
(45) Hao, L. T.; Park, S.; Choy, S.; Kim, Y.-M.; Lee, S.-W.; Ok, Y. S.; Koo, J. M.; Hwang, S. Y.; Hwang, D. S.; Park, J.; Oh, D. X. Strong, Multifaceted Guanidinium-Based Adhesion of Bioorganic Nanoparticles to Wet Biological Tissue. *JACS Au* **2021**, *1* (9), 1399−1411.
(46) Ahn, B. K.; Das, S.; Linstadt, R.; Kaufman, Y.; Martinez-Rodriguez, N. R.; Mirshafian, R.; Kesselman, E.; Talmon, Y.; Lipshutz, B. H.; Israelachvili, J. N.; Waite, J. H. High-Performance Mussel-Inspired Adhesives of Reduced Complexity. *Nat. Commun.* **2015**, *6* (1), 8663.
(47) Lou, J.; Mooney, D. J. Chemical Strategies to Engineer Hydrogels for Cell Culture. *Nat. Rev. Chem.* **2022**, *6* (10), 726−744.
(48) Chamchoy, K.; Pakotiprapha, D.; Pumirat, P.; Leartsakulpanich, U.; Boonyuen, U. Application of WST-8 Based Colorimetric NAD(P)H Detection for Quantitative Dehydrogenase Assays. *BMC Biochem.* **2019**, *20* (1), 4.
(49) Hughes, C. S.; Postovit, L. M.; Lajoie, G. A. Matrigel: a Complex Protein Mixture Required for Optimal Growth of Cell Culture. *Proteomics* **2010**, *10* (9), 1886−1890.
(50) Yin, J.; Yan, M.; Wang, Y.; Fu, J.; Suo, H. 3D Bioprinting of Low-Concentration Cell-Laden Gelatin Methacrylate (GelMA) Bioinks with a Two-Step Cross-Linking Strategy. *ACS Appl. Mater. Interfaces* **2018**, *10* (8), 6849−6857.
(51) Kilic Bektas, C.; Hasirci, V. Cell Loaded 3D Bioprinted GelMA Hydrogels for Corneal Stroma Engineering. *Biomater. Sci.* **2020**, *8* (1), 438−449.
(52) Isaacson, A.; Swioklo, S.; Connon, C. J. 3D Bioprinting of a Corneal Stroma Equivalent. *Exp. Eye Res.* **2018**, *173*, 188−193.
(53) Torgan, C. E.; Daniels, M. P. Regulation of Myosin Heavy Chain Expression During Rat Skeletal Muscle Development In Vitro. *Mol. Biol. Cell* **2001**, *12* (5), 1499−1508.
(54) Roman, W.; Gomes, E. R. Nuclear Positioning in Skeletal Muscle. *Semin. Cell Dev. Biol.* **2018**, *82*, 51−56.
(55) Cristancho, A. G.; Lazar, M. A. Forming Functional Fat: a Growing Understanding of Adipocyte Differentiation. *Nat. Rev. Mol. Cell Biol.* **2011**, *12* (11), 722−734.
(56) The Good Food Institute (GFI). *Deep Dive: Cultivated Meat Cell Lines*. https://gfi.org/science/the-science-of-cultivated-meat/deep-dive-cultivated-meat-cell-lines/ (accessed 2025-04-01).
(57) Yuen, J. S. K., Jr; Saad, M. K.; Xiang, N.; Barrick, B. M.; DiCindio, H.; Li, C.; Zhang, S. W.; Rittenberg, M.; Lew, E. T.; Zhang, K. L.; Leung, G.; Pietropinto, J. A.; Kaplan, D. L. Aggregating In Vitro-Grown Adipocytes to Produce Macroscale Cell-Cultured Fat Tissue with Tunable Lipid Compositions for Food Applications. *eLife* **2023**, *12*, No. e82120.
(58) Gebhardt, S. E.; Thomas, R. G. *Nutritive Value of Foods; Nutrient Data Laboratory, Agricultural Research Service*. US Department of Agriculture: Beltsville, MD, 2002.
(59) US Food & Drugs Administration (FDA), *Daily Value on The Nutrition and Supplement Facts Labels*. https://www.fda.gov/food/nutrition-facts-label/daily-value-nutrition-and-supplement-facts-labels (accessed 2025-04-01).
(60) DeMerlis, C. C.; Schoneker, D. R. Review of the Oral Toxicity of Polyvinyl Alcohol (PVA). *Food Chem. Toxicol.* **2003**, *41* (3), 319−326.
(61) US Food and Drugs Administration. *GRAS Notices—GRN No. 443: Shrimp-Derived Chitosan*. https://www.cfsanappsexternal.fda.gov/scripts/fdcc/?set=GRASNotices&id=443 (accessed 2025-04-01).
(62) EFSA Panel on Food Additives and Nutrient Sources added to Food (ANS). Scientific Opinion on the Re-Evaluation of Boric Acid (E 284) and Sodium Tetraborate (Borax) (E 285) as *Food Additives. EFSA J.* **2013**, *11* (10), 3407. .
(63) Scott, H.; Walmsley, R. M. Ames Positive Boronic Acids Are Not All Eukaryotic Genotoxins. *Mutat. Res. Genet. Toxicol. Environ. Mutagen.* **2015**, *777*, 68−72.
(64) Masuda-Herrera, M. J.; Dobo, K. L.; Kenyon, M. O.; Kenny, J. D.; Galloway, S. M.; Escobar, P. A.; Reddy, M. V.; Jolly, R. A.; Trejo-Martin, A.; Brown, C.; Mckeon, M.; Young, M.; Bruce, S.; Pant, K.; Dutta, A.; Kulkarni, R.; Bercu, J. P. In Vivo Mutagenicity Testing of Arylboronic Acids and Esters. *Environ. Mol. Mutagen.* **2019**, *60* (9), 766−777.
(65) Hadrup, N.; Frederiksen, M.; Sharma, A. K. Toxicity of Boric Acid, Borax and Other Boron Containing Compounds: a Review. *Regul. Toxicol. Pharmacol.* **2021**, *121*, No. 104873.
(66) US National Institutes of Health, Office of Dietary Supplements *Boron: Fact Sheet for Health Professionals*. https://ods.od.nih.gov/factsheets/Boron-HealthProfessional/ (accessed 2025-04-01).
(67) Herz, E.; Moll, P.; Schmitt, C.; Weiss, J. Binders in Foods: Definition, Functionality, and Characterization. *Food Hydrocoll.* **2023**, *145*, No. 109077.
(68) Rosales, A. M.; Anseth, K. S. The Design of Reversible Hydrogels to Capture Extracellular Matrix Dynamics. *Nat. Rev. Mater.* **2016**, *1* (2), 15012.
(69) Brunetti, J.; Koenig, S.; Monnier, A.; Frieden, M. Nanopattern Surface Improves Cultured Human Myotube Maturation. *Skelet. Muscle* **2021**, *11* (1), 12.

https://doi.org/10.1021/acsami.5c03479
ACS Appl. Mater. Interfaces 2025, 17, 31881−31897